Y161F)—heme solutions to O_2, the UV—vis absorptions immediately changed to that of the O_2 adduct complex at 0—25 °C (Figure 3).[28,29] After flowing CO gas, these hemoproteins produced stable carbonyl complexes.

The MCD spectra of the deoxy and carbonyl rHSA(I142H/Y161L)—heme are shown in Figure 4a. The Soret MCD of the deoxy state under anaerobic conditions is dominated by an intense positive peak at 435 nm, as would be expected for the Faraday C terms anticipated for the high-spin Fe^{2+} porphyrin.[20a,26] On the other hand, the rHSA(I142H/Y161L)CO exhibited S-shaped MCDs which correspond to the A term bands for the diamagnetic Fe^{2+} porphyrin.[20a,26] These spectra are very similar to those of the high-spin deoxy Mb and low-spin MbCO measured in identical conditions (Figure 4b). Our MCD results clearly show that the central ferrous ion of the heme is coordinated by His-142 in the heme pocket and forms a five-N-coordinate high-spin complex under an Ar atmosphere, which converts to the low-spin diamagnetic form by the binding of CO. The rHSA(I142H/Y161F)—heme complex had the same MCD spectral features as rHSA(I142H/Y161L)—heme (data not shown).

The single mutant rHSA(I142H)—heme complex, which retains Y161, could not bind O_2. The polar phenolate residue at the top of the porphyrin plane is likely to accelerate the proton-driven oxidation of the Fe^{2+} center. This rapid autoxidation is also observed in the rMb(H64Y) mutants, in which the distal histidine (His-64) was substituted with Tyr, thus introducing a potentially anionic nucleophile near to the O_2 coordination site.[31] In contrast, replacement of Tyr-161 in rHSA(I142H)—heme by Leu or Phe enhanced the stabilization of the O_2 adduct complex. In the rHSA(Y161L/L185H)—heme, the proximal histidine coordinated to the central ferrous ion from the opposite side of the porphyrin platform also allows O_2 binding to the heme. The lifetimes for the decays of the dioxygenated rHSA(I142H/Y161L)—heme, rHSA(I142H/Y161F)—heme, and rHSA(Y161L/L185H)—heme are all 3—5 min at 20 °C.

To evaluate the kinetics of the O_2 and CO bindings to the rHSA(mutant)—heme, laser flash photolysis experiments were carried out.[14,15] The transient absorption spectra of the photodissociated product of the rHSA(I142H/Y161L)—hemeCO displayed a negative absorbance at 417 nm, due to the disappearance of the carbonyl complex, and a positive absorbance at 435 nm, which is attributed to the deoxy form (Figure 5). The transient absorption spectra in the time range from 0.1 μs to 8.0 ms with an isosbestic point at 401, 426, and 458 nm were superimposed on the static difference spectrum of the deoxy minus carbonyl compound (Figure 5, red line). They illustrate the process of reassociation of CO and are consistent with the formation of the ferrous five-N-coordinate high-spin complex after the laser pulse irradiation.

It is noteworthy that the absorbance decays accompanying the CO recombinations to these rHSA(mutant)-heme were composed of double-exponential profiles, which are normally not observed in Mb (Figure 6a). The ratio of the amplitude of the fast and slow phases was approximately 3:2 for the rHSA-(I142H/Y161L)-heme, 5:1 for the rHSA(I142H/Y161F)-heme and 3:1 for the rHSA(Y161L/L185H)-heme. On the other hand,
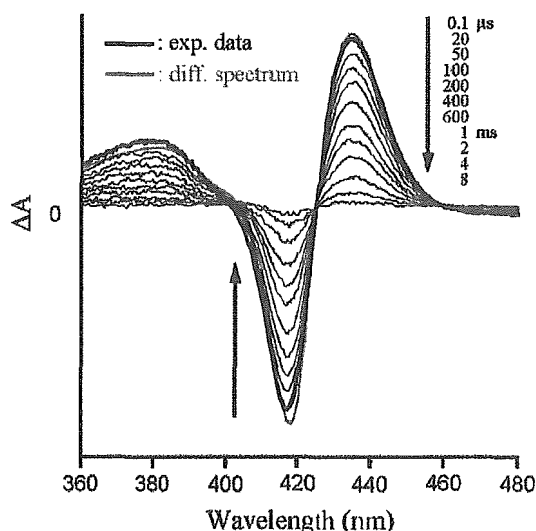

Figure 5. Transient absorption spectra of the photodissociated product of the rHSA(I142H/Y161L)-hemeCO after the laser flash photolysis at 22 °C. The red-line represents the static spectrum of deoxy minus carbonyl compound in Figure 3a.
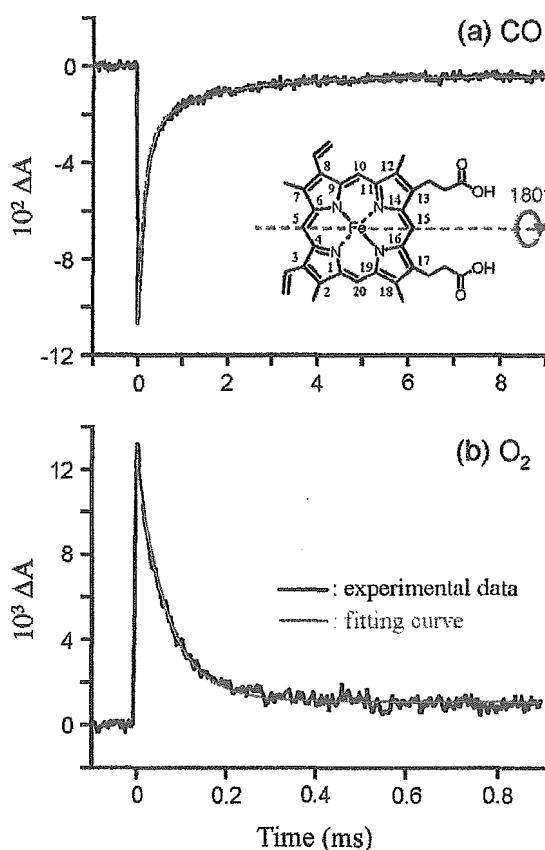

Figure 6. Absorption decay of CO rebinding to the rHSA(I142H/Y161F)-heme after the laser flash photolysis at 22 °C; the kinetics was composed of two phases and relaxation curve was fitted by double-exponentials. (b) Absorption decay of O_2 rebinding to the rHSA(I142H/Y161F)-heme after the laser flash photolysis at 22 °C; the kinetics was fitted by single-exponential relaxation curve.

the rebinding of O_2 to the rHSA(mutant)-heme followed a simple monophasic decay (Figure 6b). From numerous investigations on synthetic model hemes, it has been shown that a bending

(30) The spectra of Mb are consistent with other results reported elsewhere; refs 20, 26.
(31) Springer, B. A.; Egeberg, K. D.; Sliger S. G.; Rohlfs, R. J.; Mathews, A. J.; Olson, J. S. *J. Biol. Chem.* **1989**, *264*, 3057—3060.
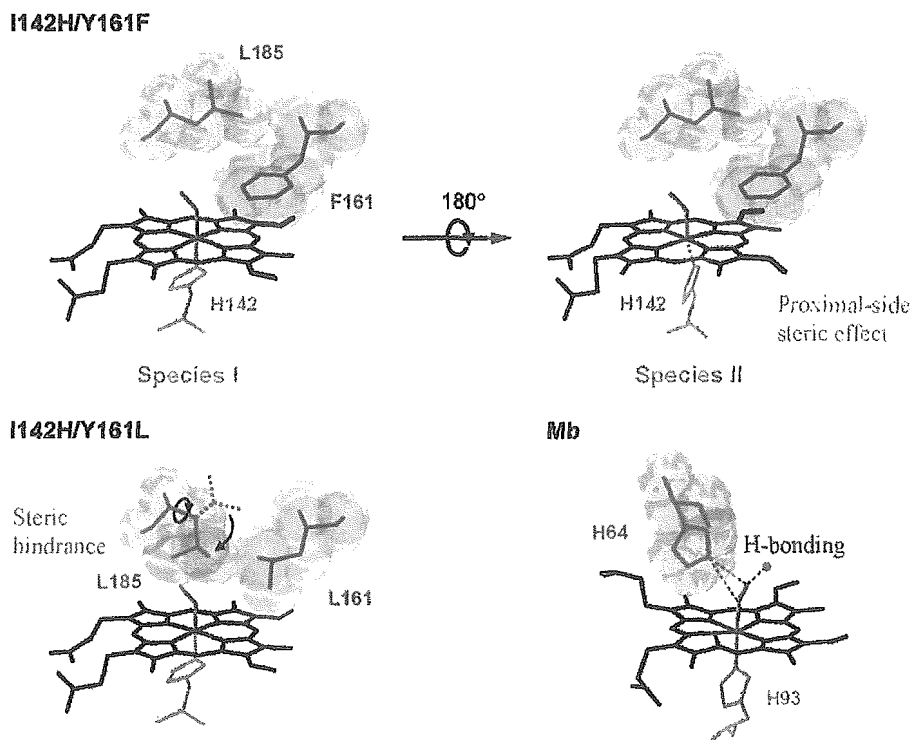
Figure 7. Structural models of the hemeO$_2$ sites of rHSA(I142H/Y161F)-heme and rHSA(I142L/Y161L)-heme, and comparison to Mb.[12,32]

strain in the proximal base coordination to the central Fe^{2+} atom, the "proximal-side steric effect", can both increase the dissociation rate and decrease the association rate for CO, whereas it increases the O$_2$ dissociation rate without greatly altering the kinetics of O$_2$ association.[14,15] One possible explanation is that there may be two different geometries of the axial histidine (His-142 or His-185) coordination to the central ferrous ion of the heme, each one accounting for a component of the biphasic kinetics of CO rebinding. Marden and co-workers also reported a similar two-phase kinetics in CO association with HSA-heme and interpreted it as indicating that there are two different orientations of the porphyrin ring in a single site on HSA.[10] In our case, the alternative geometries may arise because crystallographic analysis suggests that the heme molecule appears able to bind into the narrow cavity of subdomain IB in two orientation that are related by a 2-fold rotation about the 5,15-*meso* axis of the heme (180° rotational isomers). It appears that the asymmetric hydrophobic 3,8-divinyl groups at the porphyrin periphery may occupy different positions that result in a shift of the Fe^{2+} center, forming the two different geometries of the axial imidazole coordination of histidine (Figure 7).

In general, the crystal structures of natural hemoproteins have shown that the prosthetic heme group is bound in a single orientation. On the other hand, in solution, ^{1}H NMR spectra frequently exhibit two sets of heme (or hemin) resonances, which arise from alternative orientations of the porphyrin plane.[33] This orientational disorder is most readily detected in the ferric low-spin state, which shows extraordinary porphyrin

2,7,12,18-CH$_3$ contact shifts.[34] The amount of the minor species ranges from a few percent in Mb to 40% in insect Hb (*CTT* HbIII).[35] Reconstitution techniques have made significant contributions to clarify this molecular equilibrium; the heme in Hb and Mb can be easily removed under acidic conditions and the resulting apoprotein may be reconstituted by adding back the heme to produce the holoprotein.[36] The incorporation of hemin into apoMb is complete within 1 ms, but the initial complex does not distinguish the two possible orientations of the porphyrin ring.[34] As a result, freshly reconstituted Mb contains an equimolar 1/1 mixture of the two conformers; subsequent heme rearrangement is extremely slow ($\approx$13 h). The influence of the heme orientation on the functional properties appears to be very dependent on the particular protein. In *CTT* HbIII, the O$_2$ binding affinity depends on the heme orientation.[37] On the other hand, the equilibrium and kinetic parameters for O$_2$ and CO binding to the reconstituted human Mb are unaffected by the slow heme rearrangement.[38,39]

Our attempts to determine the ratio of the two hemin orientations of the rHSA(I142H/Y161L)-hemin by ^{1}H NMR spectroscopy unfortunately failed. The downfield spectra of the

(32) The model of Mb was prepared on the basis of crystal structure coordinate of MbO$_2$ (code: 1MBO, Phillips, S. E. *J. Mol. Biol.* **1980**, *142*, 531–554.). The coordinated O$_2$ shows a hydrogen bond with N$_ε$(His-64) and hydrogen bond network through H$_2$O (light-blue circle) within the distal pocket.

(33) La Mar, G. N.; Satterlee, J. D.; de Ropp, J. S. Nuclear Magnetic Resonance of Hemoprotein. In *The Porphyrin Handbook*; Kadish, K. M., Smith, K. M., Guilard, R., Eds.; Academic Press: San Diego, 2000; Vol. 5, pp 185–298.
(34) (a) Jue, T.; Krishnamoorthi, R.; La Mar, G. N. *J. Am. Chem. Soc.* **1983**, *105*, 5701–5703. (b) La Mar, G. N.; Toi, H, Krishnamoorthi, R, *J. Am. Chem. Soc.* **1984**, *106*, 6395–6401.
(35) (a) La Mar, G. N.; Davis, N. L.; Parish, D. W.; Smith, K. M. *J. Mol. Biol.* **1983**, *168*, 887–896. (b) La Mar, G. N.; Smith, K. M.; Gersonde, K.; Sick, H.; Overcamp, M. *J. Biol. Chem.* **1980**, *255*, 66–70.
(36) Hayashi, T.; Hisaeda, Y. *Acc. Chem. Res.* **2002**, *35*, 35–43.
(37) Gersonde, K.; Sick, H.; Overkamp, M.; Smith, K. M.; Parish, D. W. *Eur. J. Biochem.* **1986**, *157*, 393–404.
(38) Light, W. R.; Rohlfs, R. J.; Palmer, G.; Olson, J. S. *J. Biol. Chem.* **1987**, *262*, 46–52.
(39) Aojula, H. S.; Wilson, M. T.; Morrison, I. G.*Biochem. J.* **1987**, *243*, 205–210.

Table 2. O_2 Binding Parameters of the rHSA(mutant)-Heme in 50 mM Potassium Phosphate Buffer Solution (pH 7.0) at 22 °C[a]

Hemoproteins	$k_{on}{}^{O_2}$ ($\mu M^{-1} s^{-1}$)	$k_{off}{}^{O_2}$ (ms^{-1}) I	II	$P_{1/2}{}^{O_2}$ (Torr) I	II
rHSA(I142H/Y161L)-Heme	7.5	0.22	1.7	18	134
rHSA(I142H/Y161F)-Heme	20	0.10	0.99	3	31
rHSA(Y161L/L185H)-Heme	31	0.20	2.1	4	41
Hbα (R-state)[b]	33[c]	0.013[d]		0.24	
Mb[e,f]	14	0.012		0.51	
rMb(H64L)[f]	98	4.1		26	
rMb(H64F)[f]	75	10		82	
RBC[g]				8	

[a] Number I or II indicates species I or II. [b] Human Hb α-subunit. [c] In 0.1 M phosphate buffer (pH 7.0, 21.5 °C); ref 40. [d] In 50 mM phosphate buffer (pH 7.0, 20 °C); ref 41. [e] Sperm whale Mb. [f] In 0.1 M potassium phosphate buffer (pH 7.0, 20 °C); ref 16. [g] Human red cell suspension. In isotonic buffer (pH 7.4, 20 °C); ref 42.

Table 3. CO Binding Parameters of the rHSA(mutant)-Heme in 50 mM Potassium Phosphate Buffer Solution (pH 7.0) at 22 °C[a]

Hemoproteins	$k_{on}{}^{CO}$ ($\mu M^{-1} s^{-1}$) I	II	$k_{off}{}^{CO}$ (s^{-1}) I	II	$P_{1/2}{}^{CO}$ (Torr) I	II
rHSA(I142H/Y161L)-Heme	2.0	0.27	0.013	0.079	0.0053	0.24
rHSA(I142H/Y161F)-Heme	6.8	0.72	0.009	0.061	0.0011	0.068
rHSA(Y161L/L185H)-Heme	3.7	0.35	0.012	0.077	0.0026	0.18
Hbα (R-state)[b]	4.6[c]		0.009[d]		0.0016[e]	
Mb[f,g]	0.51		0.019		0.030	
rMb(H64F)[g]	4.5		0.054		0.0097	

[a] Number I or II indicates species I or II. [b] Human Hb α-subunit. [c] In 50 mM potassium phosphate buffer (pH 7.0, 20 °C); ref 45. [d] In 0.1 M phosphate buffer (pH 7.0, 20 °C); ref 44. [e] Calculated from $k_{on}{}^{CO}/k_{off}{}^{CO}$. [f] Sperm whale Mb. [g] In 0.1 M potassium phosphate buffer (pH 7.0, 20 °C); refs 16, 48.

rHSA(I142H/Y161L)-hemin did not show sharp resonances of the four porphyrin CH_3 groups. Other trials to convert the rHSA-(I142H/Y161L)-hemin in the low-spin azide adduct complex,[33] which is much better suited for the ^1H NMR investigation, also failed even with the addition of a large excess of ligand. In any case, the amplitude ratio of the two phases observed for the CO association to rHSA(mutant)-heme was always the same, independent of time after preparation.

O_2 and CO Binding Parameters. By analyzing the CO/O_2 competitive binding following laser flash photolysis,[14,15] we obtained the association rate constants for O_2 ($k_{on}{}^{O_2}$) and the O_2 binding affinities [$P_{1/2}{}^{O_2} = (K^{O_2})^{-1}$] for the rHSA(I142H/Y161L)-heme, rHSA(I142H/Y161F)-heme and rHSA(Y161L/L185H)-heme (Table 2). From eq 6, variation in $k_{on}{}^{CO}$ arising from the two geometries of the His coordination (the faster phase is defined as species I and the slower phase is defined as species II) yielded two different O_2 binding affinities. In species I, the proximal His may coordinate to the central ferrous ion without strain, whereas in species II, the ligation may involve some distortion, resulting in weaker O_2 binding (Figure 7). The absorbance decay accompanying the CO dissociation from the rHSA(mutant)-hemeCO by the replacement with NO also showed double-exponential profiles, giving two values of $k_{off}{}^{CO}$ (Table 3). The proximal-side steric effect generally increases the dissociation rate for CO,[14,15] a result that is quite consistent with our interpretation that there are two orientation isomers of the heme (the larger component of $k_{off}{}^{CO}$ originating from species II).

The $P_{1/2}{}^{O_2}$ values of the rHSA(mutant)-heme were determined to be 3−18 and 31−134 Torr for species I and II, respectively. Thus even the O_2 binding affinities of species I were 6−75-

fold lower than those of native Hbα (R-state) and Mb.[16,40–42] Kinetically, these low affinities for O_2 were due to an 8−18-fold increase in the O_2 dissociation rate constants. Neutron diffraction studies of MbO_2 revealed that there is a direct hydrogen bond between the distal His-64 and the coordinated O_2 (Figure 7).[43] The high-resolution X-ray crystallographic structure of $HbαO_2$ also suggested a similar interaction in the heme pocket.[44] In both hemoproteins, the distal His stabilizes the bound O_2 by about −1.4 kcal mol^{-1} due to the hydrogen bonding. On the basis of the mutagenesis studies on sperm whale rMb, Rohlfs and co-workers demonstrated that the replacement of His-64 with apolar amino acid residues (Leu or Phe) results in loss of the hydrogen bonding, and markedly increased the O_2 dissociation rates (342−833-fold higher than Mb).[16] In the rHSA(mutant)-heme, the dioxygenated heme is buried in the core of the hydrophobic cavity without any counterpart for the hydrogen bond; thus the even small $k_{off}{}^{O_2}$ values for species I are greater than those of Hbα and Mb. In species II, the proximal-side steric effect could further increase the dissociation rates and cause a large decline in the O_2 binding affinity. In contrast, the binding parameters of CO to the rHSA(mutant)-heme (species I) exhibited similar values of Hbα ($\leq$3-fold),[45,46] because the coordinated CO in Hbα does not form a hydrogen bond with the distal His-64.[47]

Comparison of the O_2 binding parameters for rHSA(I142H/Y161L)-heme and rHSA(I142H/Y161F)-heme shows that the presence of a Phe rather than Leu at position 161 results in 6-fold and 4-fold increases in the O_2 binding affinity for species I and II, respectively. This is mainly due to an increase in the O_2 association rate constant (Table 2). The same trend was observed for CO binding (3-fold increase in $k_{on}{}^{CO}$) (Table 3). The substitution of Leu-161 (102 Å^3) by Phe-161 (137 Å^3)[49] replaces an isopropyl group with a rigid benzyl group within the heme pocket. In I142H/Y161L, the small side-chain of Leu-161 may allow free rotation of the side-chain of neighboring Leu-185, thereby reducing the volume on the distal-side of the porphyrin plane (Figure 7). Actually, modeling and experimental studies suggest that His-185 in Y161L/L185H can coordinate to the central ferrous ion of the heme. On the other hand, the bulkier aromatic side-chain of Phe-161 may prevent rotation of the isopropyl group of Leu-185 and thereby provide greater room of the distal pocket; this might allow easier access to the heme Fe atom and account for the increased association rates for O_2 and CO.

Conclusion

HSA exploits weak axial coordination by Tyr-161 to bind hemin into the heme pocket. Reduction of the central ferric ion partly disrupts the Fe−O(phenolate) bond and produces unusual

(40) Gibson, Q. H. J. Biol. Chem. 1970, 245, 3285−3288.
(41) Olson, J. S.; Andersen, M. E.; Gibson, Q. H. J. Biol. Chem. 1971, 246, 5919−5923.
(42) Imai, K.; Morimoto, H.; Kotani, M.; Watari, H.; Hirata, W.; Kuroda, M. Biochim. Biphys. Acta 1970, 200, 189−197.
(43) Phillips, S. E. V.; Schoenborn, B. P. Nature 1981, 292, 81−82.
(44) Shaanan, B. J. Mol. Biol. 1983, 171, 31−59.
(45) Steinmeier, R. C.; Parkhurst, L. J. Biochemistry 1975, 14, 1564−1571.
(46) Sharma, V. S.; Schmidt, M. R.; Ranney, H. M. J. Biol. Chem. 1976, 251, 4267−4272.
(47) Hanson, J. C.; Schoenborn, B. P. J. Mol. Biol. 1981, 153, 117−146.
(48) rMb(H64L) exhibited an abnormally large CO binding affinity and $k_{on}{}^{CO}$ compared to those of other mutants; ref 16.
(49) Creighton, T. E. Proteins: Structures and Molecular Properties; W. H. Freeman and Co.: New York, 1983; p 242.

ferrous four-coordinate intermediate-spin state hemoprotein. We have engineered mutant rHSA-heme complexes which can bind O_2 reversibly with an affinity that is only 1 order of magnitude lower than the affinity of O_2 for Hbα (R-state) and Mb. The principal modifications to the heme pocket that are required to confer reversible O_2 binding are (1) replacement of Tyr-161, the endogenous anionic nucleophile, by hydrophobic amino acid (Leu or Phe), and (2) introduction of His as a proximal base at position Ile-142 or Leu-185 (either side of the porphyrin ring plane). The transport of O_2 by the rHSA-heme could be of tremendous clinical importance not only as a red cell substitute but also as an O_2-providing therapeutic reagent. Although a number of Hb-based O_2 carriers have already been developed, the administration of these materials often elicits an acute increase in blood pressure by vasoconstriction.[50–52] This side-effect is caused by the rapid capture of the endothelial-derived relaxing factor, namely NO, by Hb that has leaked through the vascular endothelium. In contrast, our rHSA(mutant)-heme would not induce such hypertension, because the albumin carrier has low permeability through the muscle capillary pore.[53]

Our results on several mutants have also shown that modification of the distal-side of the heme pocket has a measurable effect on O_2 binding affinity (compare Leu-161 and Phe-161). To develop this promising O_2 carrier as a blood substitute, further work using a combined mutagenic and synthetic approach is required; (1) additional mutations, e.g. an introduction of a distal base which in Mb and Hbα forms a hydrogen bond with the coordinated O_2, may help to stabilize the O_2 adduct complex, and (2) small modifications to the heme structure designed to adjust its position within the pocket interior but without straining the proximal His coordination, may improve and modulate the O_2 binding ability. To aid these modifications, crystal structural analysis of rHSA(mutant)-heme complexes is now underway.

Supporting Information Available: UV−vis absorption and MCD spectra of FePPIXDME, MCD spectra of the ferric rHSA-(mutant)-hemin and aquo-metMb. This material is available free of charge via the Internet at http://pubs.acs.org.

JA054819U

(50) Tsuchida, E. Perspectives of Blood Substitutes. In*Blood Substitutes: Present and Future Perspectives*; Tsuchida, E., Ed.; Elsevier Science: Lausanne, 1998; pp 1−14.
(51) Winslow, R. M. *Annu. Rev. Med.* **1999**, *50*, 337−353.
(52) Squires, J. E. *Science* **2002**, *295*, 1002−1005.
(53) Tsuchida, E.; Komatsu, T.; Matsukawa, Y.; Nakagawa, A.; Sakai, H.; Kobayashi, K.; Suematsu, M. *J. Biomed. Mater. Res.* **2003**, *64A*, 257−261.

Albumin Clusters: Structurally Defined Protein Tetramer and Oxygen Carrier Including Thirty-Two Iron(II) Porphyrins

Teruyuki Komatsu,* Yukiko Oguro, Akito Nakagawa, and Eishun Tsuchida*

Advanced Research Institute for Science and Engineering, Waseda University, 3-4-1 Okubo,Shinjuku-ku, Tokyo 169-8555, Japan

Recombinant human serum albumin (rHSA) clusters have been synthesized and physicochemically characterized. Cross-linking between the Lys groups of the core albumin and a unique Cys-34 of the shell albumins with an *N*-succinimidyl-6-[3′-(2-pyridyldithio)propionamido]hexanoate produced the structurally defined rHSA trimer and tetramer. MALDI-TOF—MS showed a single peak with the triple and quadruple masses of rHSA. Their molar ellipticities and the isoelectric points (pI = 4.8) are all identical to those of the monomer, suggesting that the essential structures of the albumin units were intact. TEM observations demonstrated a uniform morphology of the rHSA tetramer with a diameter of 20—30 nm. The circulation half-life ($\tau_{1/2}$) of the ^{125}I-labeled rHSA tetramer in rat (5.5 h) was significantly longer than that of the monomer (2.3 h) due to the low ratio of the distribution phase (α-phase). A total of 24 and 32 molecules of the synthetic iron(II) porphyrins (FePs) are incorporated into the hydrophobic cavities of the rHSA trimer and tetramer, respectively, producing huge artificial hemoproteins. These albumin—heme clusters can reversibly bind and release O_2 under physiological conditions (37 °C, pH 7.3) and showed similar O_2-binding properties (O_2-binding affinity, association and dissociation rate constants) to those of the corresponding monomer. A large volume of O_2 can be chemically dissolved into the albumin—heme cluster solutions relative to the monomeric rHSA-FeP when the molar concentration of the albumin scaffold is identical.

Introduction

In our bloodstream, hydrophobic molecules of medium size (ex., long-chain fatty acids, bilirubin, steroids, hemin) are captured by human serum albumin (HSA, Mw: 66.5 kDa) and are allowed to circulate for a relatively long time to reach the disposal sites in the body.[1] The transporting ability of this shuttle protein contributes to maintaining the high concentration levels of the therapeutic drugs in the circulatory system.[1,2] Moreover, the albumin peptide exhibited a slow terminal clearance and catabolism, so that the conjugation of HSA with a therapeutic protein (ex., soluble CD4 and interferon-α) provides clinical benefits in permitting less frequent administrations.[3] We have found that synthetic iron(II) porphyrins (hemes) were incorporated into the hydrophobic cavities of HSA, producing an albumin—heme hybrid, which can reversibly bind and release dioxygen (O_2) under physiological conditions (pH 7.3, 37 °C).[4] This artificial hemoprotein has the capability to carry O_2 like hemoglobin (Hb) or myoglobin (Mb) and functions as a red blood cell (RBC) substitute in vivo.[5]

One of the interesting characteristics of the HSA structure is the presence of a single reactive thiol of Cys-34.[1,6] The reaction of the bifunctional reagent, 1,6-bis(maleimido)-hexane (BMH), with HSA successfully creates an intermolecular covalent bridge between the two Cys-34s.[7] A total

of 16 molecules of synthetic heme were accommodated into the dimer and the obtained albumin—heme dimer solution is able to transport a large volume of O_2 compared to the human blood ([heme] = 9.2 mM) while maintaining the colloid osmotic pressure on a physiological level.[7b] Another remarkable advantage of the HSA dimer is its long circulation persistence relative to the monomer, since the 2× size of the molecule could serve to remain in the blood vessel. We now extend this approach to produce the structurally defined albumin trimer and tetramer, namely "albumin clusters". In this paper, we report, for the first time, the synthesis, physicochemical characterization, and preliminary pharmacokinetics of the albumin clusters cross-linked by *N*-succinimidyl-6-[3′-(2-pyridyldithio)propionamido]hexanoate (SP-DPH), which efficiently connects an NH_2 group of Lys and an SH group of Cys. The O_2-binding properties of the albumin—heme clusters incorporating the 2-[8-{*N*-(2-methylimidazolyl)}octanoyloxymethyl]-5,10,15,20-tetrakis{α,α,α,α-*o*-(1-methylcyclohexanamido)phenyl}porphinatoiron(II) (FeP, Scheme 1), are also evaluated and compared to those of the corresponding monomer.

Experimental Section

Materials and Apparatus. An rHSA (Albrec, 25 wt %) was provided from the NIPRO Corp (Osaka, Japan). Ethanol, dithiothreitol, and 2,2′-dithiopyridine (all high-purity grades) were purchased from Kanto Chemical Co., Inc. (Tokyo) and used without further purification. *N*-Succinimidyl-6-[3′-(2-pyridyldithio)propionamido]hexanoate (SPDPH) was

* To whom correspondence should be addressed. Prof. Eishun Tsuchida, Ph.D. Tel: +81-3-5286-3120. Fax: +81-3-3205-4740. E-mail: eishun@waseda.jp (Eishun Tsuchida). E-mail: teruyuki@waseda.jp (Teruyuki Komatsu).

Scheme 1
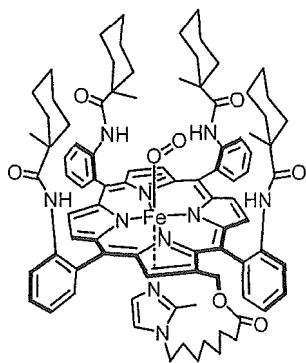
purchased from Pierce Biotechnology (Rockford, USA). 2-[8-{*N*-(2-Methylimidazolyl)}octanoyloxymethyl]-5,10,15,20-tetrakis{α,α,α,α-*o*-(1-methylcyclohexanamido)-phenyl}porphinatoiron(II) (FeP) was prepared according to our previously reported procedure.[8]

Synthesis of rHSA Clusters. Ethanolic SPDPH (20 mM, 0.75 mL) was slowly added dropwise into the rHSA solution (0.75 mM, 2.0 mL) and gently stirred for 20 min at room temperature. The reaction mixture was diluted with phosphate-buffered saline (PBS, 10 mM, pH 7.4, 25 mL) and concentrated to 2.5 mL using an ADVANTEC UHP-76K ultrafiltration system with a Q0500 076E membrane (cutoff Mw 50 kDa). This washing was repeated three times to remove the excess SPDPH, affording 3'-(2-pyridyldithio)propionamido]hexanoated albumin (PDPH—rHSA, [rHSA] = 5.15 wt %, 2 mL). The albumin concentrations were normally measured by bromcresol green (BCG) methods using a Wako AlbuminB—Test.[9] The number of PDPH chains introduced into rHSA was determined by the assay of 2-thiopyridinone (2TP) with an absorption at 343 nm [molar absorption coefficient (ϵ_{343}): 8.1 × 10³ M⁻¹cm⁻¹]. A 15-fold molar excess of dithiothreitol (DTT, 1 M, 1.35 μL) was added to the PBS solution of PDPH—rHSA (30 μM), and the formed 2-TP was quantitatively assayed after 10 min.

On the other hand, aqueous DTT (1.0 M, 56 μL) was added to the phosphate-buffered solution (pH 7.0, 10 mM) of rHSA (0.75 mM, 20 mL), and the solution was quickly mixed by a vortex mixer, followed by incubation for 30 min at room temperature. The resultant was washed three times with PBS the same as above, yielding a mercapto—albumin (SH—rHSA, 13 mL, [rHSA] = 7.77 wt %). The mercapto ratio of the Cys-34 was confirmed as 100% using the 2,2'-ditiopyridine (2,2'-DTP) procedure.[10,11]

The SH—rHSA solution was then added to the PDPH—rHSA, and the mixture was gently stirred for 20 h at room temperature. The Native-PAGEs were performed using an Amersham Biosciences Electrophoresis Power Supply EPS 301 with a PAG Mini Daiichi 2/15 (Daiichi Pure Chemicals, Co. Ltd.). The Native-PAGE pattern of the obtained reactant showed six bands including the unreacted SH—rHSA monomer. The HPLC measurement also demonstrated the formation of the rHSA clusters with a high molecular weight. The HPLC system consisted of a Shimadzu LC-8A pump and a Shimadzu SPD-10A UV detector. A Shodex Protein KW-803 column was used with PBS (pH 7.4) as the mobile phase

at 25 °C (1.0 mL min⁻¹). Peak fitting of the elution curve was done using a Hulinks PeakFit program.

The rHSA clusters were purified by gel column chromatography using a BIO-RAD EGP Combo Rec system with Superdex 200pg (Pharmacia Corp., 5 cmφ × 40 cm) and PBS (pH 7.4) as the mobile phase (3.5 mL min⁻¹). The eluant was monitored at 280 nm and fractionated by a BIO-RAD model 2110 collector. The fraction showing the single bands for band C and D in the Native-PAGE was then carefully collected. The matrix associated laser desorption ionization time-of-flight mass spectra (MALDI-TOF—MS) were obtained using a Shimadzu AXIMA-CFR Kompact MALDI. The 10 mg mL⁻¹ sinapinic acid in 40% aqueous CH₃CN was used as a matrix. The purity of the each component was checked by the HPLC measurement. The obtained yield was 10% for the rHSA trimer (band C) and 7% for the rHSA tetramer (band D).

Physicochemical Properties. The UV—vis absorption spectra were recorded on a JASCO V-570 spectrophotometer. The measurements were normally performed at 25 °C. Circular dichroism (CD) spectra were obtained using a JASCO J-725 spectropolarimeter. The concentration of the rHSA sample was 2 μM in PBS, and quartz cuvettes with a 1.0-mm thickness were used for the measurements over the range of 195—250 nm.

Transmission Electron Microscopy (TEM). An aqueous solution of the albumin cluster was mixed with 2% phosphotungstic acid (pH 7), and the droplet was placed onto a 200 mesh carbon-coated copper grid, which was hydrophilized by a JEOL HDT-400 hydrophilic treatment device prior to use. The grid was allowed to air-dry and observed in a JEOL JEM-1011 electron microscope at an accelerating voltage of 100 kV.

Circulation Lifetime in Vivo. The 125-Iodinated rHSA tetramer was prepared by our previously reported procedures.[7b] The recovered ¹²⁵I-albumin had a specific activity of 24.3 MBq mg⁻¹ and was diluted by nonlabeled albumin tetramer before administration into anesthetized Wistar rats (ca. 250 g, male). The kinetics of the albumin clearance from the circulation was monitored by measuring the radioactivity in the plasma phase of blood taken from the lateral tail veins using an Aloka ARC 2000 Autowell Gamma Counter. Acid precipitability of the recovered radioactivity was confirmed by the TCA method.[7b,12] The rats were sacrified 8 days after the sample injection by hemorrhage. The radioactivity of the excised organs was also measured. The care and handling of the animals were in accordance with NIH guidelines.

Preparation of Albumin—Heme Clusters. The preparations of albumin—heme clusters (rHSA—FeP trimer and tetramer) were carried out by mixing the EtOH solution of carbonyl—FeP and an aqueous phosphate-buffered solution of albumin clusters according to our previously reported procedures ([FeP]/[rHSA] = 26/1 or 34/1 (mol/mol)).[4a,7b,8] The albumin concentrations were measured using the CD spectra, and the amount of FeP was determined by the assay of the iron ion concentration using inductively coupled plasma spectrometry (ICP) with a Seiko Instruments SPS 7000A spectrometer.

Magnetic Circular Dichroism (MCD). MCD spectra for the phosphate-buffered solution of the albumin—heme clusters (10 μM) under N_2, CO, and O_2 atmospheres were measured using a JASCO J-820 circular dichrometer fitted with a 1.5 T electromagnet. The CD spectra at 0 T were always used as a baseline for each condition.

O_2-Binding Equilibrium and Kinetics. O_2 binding to FeP was expressed by eq 1:

$$\text{FeP} + O_2 \underset{k_{off}}{\overset{k_{on}}{\rightleftharpoons}} \text{FeP}(O_2) \quad (K = k_{on}/k_{off}) \quad (1)$$
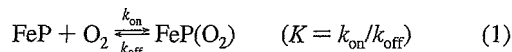
The O_2-binding affinity (gaseous pressure at half O_2 binding for heme, $P_{1/2} = 1/K$) was determined by UV—vis absorption spectral changes at various O_2 partial pressure.[4b,8,13] The appropriate O_2/N_2 gas mixture (P_{O2}: 0, 10, 20, 30, 80, 160, and 760 Torr) was prepared by a KOFLOC Gasblender GB-3C, and each spectrum was measured after flowing the gas for 15 min at 25 or 37 °C. FeP concentrations of 20 μM were normally used for the measurements in the range of 350—700 nm. The O_2-binding constant (K) was then calculated from the difference of the absorbance at 444 nm using Drago's equation.[4b,8] The half-lifetimes of the dioxygenated species of the albumin—heme clusters were determined by the time dependence of the absorption intensity for the O_2—adduct complex (549 nm).

The association and dissociation rate constants for O_2 (k_{on} and k_{off}) were measured by a competitive rebinding technique using a Unisoku TSP-1000WK—WIN time-resolved spectrophotometer with a Spectron Laser Systems SL803G-10 Q-switched Nd:YAG laser, which generated a second-harmonic (532 nm) pulse of 6-ns duration (10 Hz). A 150 W xenon arc-lamp was used as the monitor light source. The concentration of the albumin—heme cluster was normally 20 μM and experiments were carried out at 25 °C. The absorption decays accompanying the O_2 association obeyed three-component kinetics. We employed triple-exponentials equation to analyze the absorption decays; $\Delta A(t)$[4c]

$$\Delta A(t) = C_1 \exp(-k_1 t) + C_2 \exp(-k_2 t) + C_3 \exp(-k_3 t) \quad (2)$$

where k_1, k_2, and k_3 are apparent rate constants for the each components.

O_2-Concentration Measurements. The chemically dissolved O_2 in albumin—heme cluster solution was measured using an Ocean Photonics FOXY2000 Fiber Optic Oxygen Sensor with a USB2000 multichannels monochromator and FOXY-AL300 fiber optic sensor (Tokyo). This apparatus uses the fluorescence of a ruthenium complex to measure the partial pressure of O_2. The addition of 0.1 mL of CO to the phosphate-buffered solution of the dioxygenated rHSA—FeP cluster or monomer ([FeP]: 50 μM, 2.0 mL, [O_2]: 700 Torr) in the closed tube immediately dissociates the coordinated O_2 from FeP and increases the dissolved O_2 content in the aqueous phase.

Results and Discussion

Synthesis and Characterization of rHSA Clusters. We have shown that covalent cross-linking a unique Cys-34 of rHSA with BMH provided a defined rHSA dimer, in which
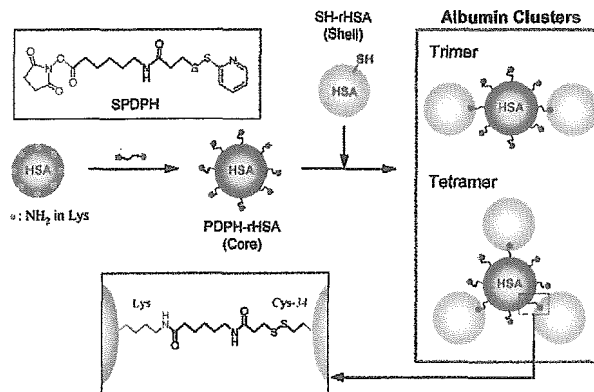

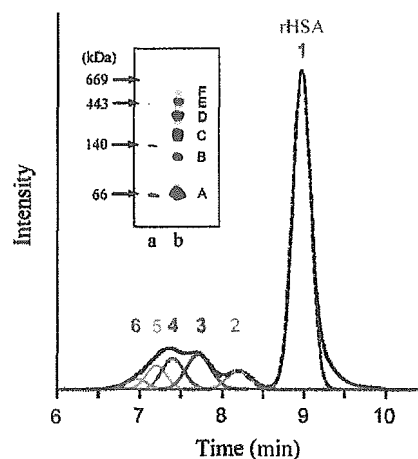**Figure 1.** Synthetic scheme of albumin clusters with SPDPH.

Figure 2. Native-PAGE electrophoresis and HPLC elution curve of the reaction mixture at 25 °C. In the Native-PAGE pattern, lane a, protein ladder; lane b, the reaction mixture (band A: rHSA monomer). The HPLC profile was simulated by a six-components model using a PeakFit (the dotted line, the sum of the simulated six components; peak 1, rHSA monomer).

the essential structures of the rHSA unit are intact.[7b] We now extend this approach to produce albumin clusters. Our first attempt to connect the Cys-34 of rHSAs by multi-armed maleimido(polyoxyethylene) unfortunately failed. The maleimido-terminate at the polyoxyethylene chains are likely to be too flexible to react with the small thiol on the large rHSA molecule to make albumin clusters. On the other hand, N-succinimidyl-6-[3'-(2-pyridyldithio)propionamido]hexanoate (SPDPH) was successfully connected to an NH_2 group of Lys and an SH group of Cys on the protein surface. Since rHSA contains 59 Lys in the globular structure, mixing a small molar excess SPDPH with rHSA immediately produced a 6-[3'-(2-pyridyldithio)propionamido]hexanoated rHSA (PDPH—rHSA; Figure 1). Assay of the pyridyldithio residues revealed that approximately 8.3 chains of PDPH were introduced into one rHSA molecule. The PDPH—rHSA acts as a core albumin for the next reaction.

Dithiothreitol (DTT) selectively reduces the mixed-disulfide of Cys-34[10,11] producing a mercapto—rHSA (SH—rHSA) as a shell albumin. After removing DTT, SH—rHSA was slowly dropwise added to the PDPH—rHSA and stirred for 20 h at room temperature (Figure 1). Native-PAGE of the reactant showed six distinct migration bands (Figure 2 inset, lane b: A—F, band A: SH—rHSA). On the basis of the
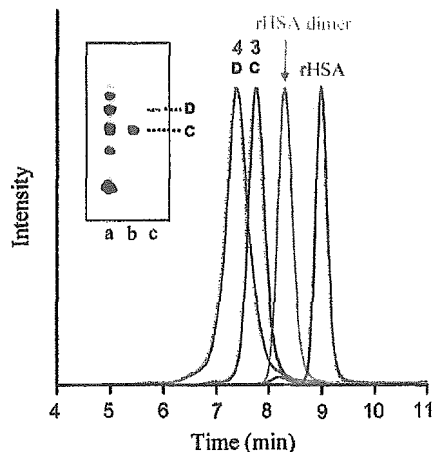
Figure 3. Native-PAGE electrophoresis and HPLC elution curves of the isolated rHSA clusters at 25 °C. In the Native-PAGE pattern, lane a, reaction mixture before purification; lane b, isolated band C; lane c, isolated band D. In the HPLC profiles, red line, rHSA monomer; orange line, rHSA dimer bridged through Cys-34 by BMH; blue line, isolated band C, which corresponds to the rHSA trimer; green line, isolated band D, which corresponds to the rHSA tetramer.

Table 1. Molecular Masses and p*I* Values of rHSA Monomer, Dimer, and Clusters

	M_w		
	obs.[a]	calcd.	p*I*
rHSA[b]	66331	66451	4.8
rHSA dimer[b,c]	132741	133180	4.8
band C (rHSA trimer)	200469	201614	4.8
band D (rHSA tetramer)	266538	267953	4.8

[a] Measured by MALDI-TOF–MS. [b] From ref 7b. [c] rHSA dimer bridged Cys-34 by BMH.

comparison with the protein ladder (lane a), the molecular weights of the bands B, C, and D were estimated to be ca. 130, 200, and 260 kDa, respectively. It can be postulated that they are the rHSA dimer, trimer, and tetramer. The pyridyldithio terminates of the core albumin reacted with the single active Cys-34 of the shell albumin creating albumin clusters. The HPLC profile of the reaction mixture exhibited broad multiple bands in the range of 6.5–8.5 min before the rHSA peak (9.0 min; Figure 2). From the careful inspection of the elution curve by peak fitting simulation, we could divide the entire pattern into six components (peaks 1–6). Most probably, the peaks 2–6 correspond to the rHSA dimer to hexamer. Gel permeation chromatography also showed a similar elution curve. Several synthesis repetitions always gave the same patterns in Native-PAGE, HPLC, and GPC. The fractions whose Native-PAGE showed bands C and D were then corrected (Figure 3, inset lanes b and c). Their HPLC profiles exhibited a sharp peak at the exactly the same position where we predicted for peaks 3 and 4 in Figure 2.

The MALDI-TOF–MS of the components of peaks 3 (band C) and 4 (band D) showed a molecular masses at m/z 200469 and 266538, respectively, which are in good agreement with the calculated value of the rHSA trimer and tetramer (M_w = 201614 and 267953) within a difference of 0.5% (Table 1). We first isolated the well-defined rHSA trimer and tetramer in which the Lys groups of the core
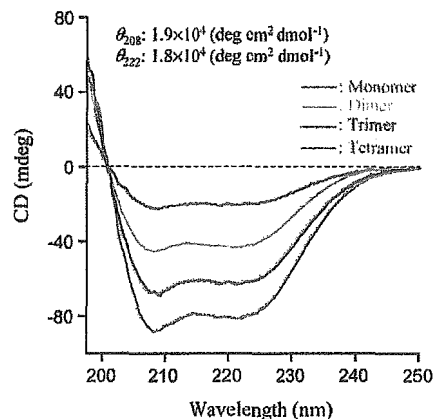
albumin are covalently bridged by the Cys-34 group of the shell albumins.

The peak area evaluations for the six components in Figure 2 indicated their molar ratios in the reaction mixture; monomer (88.2%), dimer (3.1%), trimer (4.3%), tetramer (2.5%), pentamer (1.4%), and hexamer (0.5%). Because the average degree of polymerization was 3.3, we estimated the reaction ratio (X) of the PDPH–rHSA

reacted PDPH–rHSA:unreacted (PDPH–rHSA + SH–

$$rHSA) = X:(1 - X) + (10 - 2.3X) = 11.8:88.2 \quad (3)$$

Thus, X was calculated to be 1.0; this means that all of the PDPH–rHSA (core albumin) participated in the reaction with the shell albumin. The formation ratio of each cluster can be estimated; dimer (26%), trimer (36%), tetramer (22%), pentamer (12%), and hexamer (4%).

The CD spectral patterns (λ_{min} = 208 and 222 nm) and the molar ellipticities at 208 and 222 nm ($[\theta]_{208}$ = 1.9 × 10^4 deg cm^2 dmol^{-1}, $[\theta]_{222}$ = 1.8 × 10^4 deg cm^2 dmol^{-1}) of the isolated rHSA trimer and tetramer were identical to those of the monomer and dimer (Figure 4).[4b,7b] Their isoelectric points (p*I* = 4.8) were also identical to that of rHSA (Table 1). These results implied that the secondary/tertiary structure, the α-helix content, and surface net charges of the rHSA units were intact after the cluster formation.

TEM of the negatively stained samples of the rHSA tetramer showed homogeneous particles with a diameter of 20–30 nm (Figure 5a,b). The appearance of the cluster solutions was unchanged for over one year and underwent no aggregation and precipitation. We postulate that one tetramer consists of four rHSA molecules bound in the trigonal pyramid form, which was drawn as a model in Figure 5c. rHSA involves a total of 59 Lys groups, and the cross-linker SPDPH can statistically bind to the surface. On the basis of the assay of the dithiopyridyl group, we found that the 8.3 functional PDPH arms are introduced into the core albumin. The shell albumins (SH–rHSAs) therefore approach the PDPH–rHSA from all directions to form a disulfide bridge with Cys-34. As a consequence, the conformation of the tetramer should become a trigonal pyramid-like structure, which is the most favorable arrangement to avoid the steric repulsion of the albumin units.
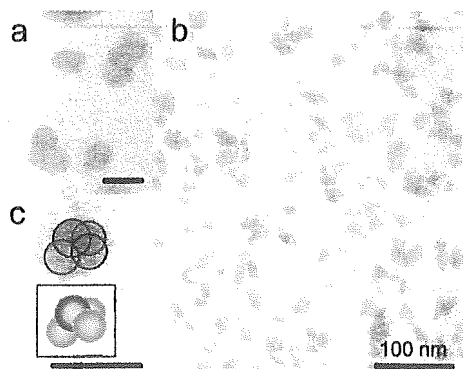

Figure 4. CD spectra of rHSA monomer, dimer bridged through Cys-34 by BMH and clusters in PBS solution (pH 7.4) at 25 °C.

Figure 5. TEM observations of negatively stained rHSA tetramer. In panels a and c, the scale bars indicate the length of 30 nm. In panel c, the trigonal pyramid form of the rHSA tetramer is predicted from the one molecule under magnification.
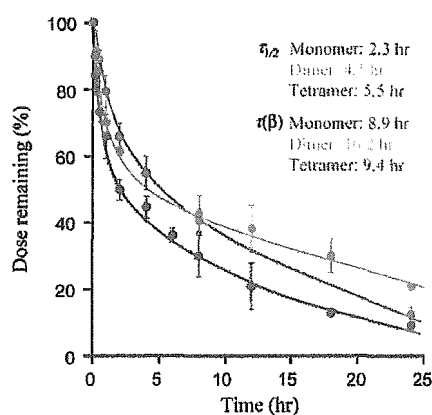

Figure 6. Plasma levels of [125]I−rHSA tetramer after intravenously administration to Wistar rats (rHSA amount = 1.0 mg kg^{-1}). The data for the [125]I−rHSA monomer and dimer were cited from our previously reported paper (ref 7b). All values are mean ± S. D. (*n* = 3).

Circulation Lifetime of ^{125}I-Labeled rHSA Tetramer in Rats. The rHSA tetramer labeled with ^{125}I was injected into anesthetized rats to determine the blood circulation lifetimes. Throughout the experiments, the turbidity of the plasma phase and the blood cell numbers were constant, showing no aggregation of the albumin clusters and blood cell components. The time courses of the radioactivity demonstrated two-phase kinetics and significant differences from the monomer's decay (Figure 6). The half-lifetime ($\tau_{1/2}$, time when the initial value decreased to 50%) of the rHSA tetramer was 5.5 h, which was 2.4-fold longer than that of the monomer (2.3 h).[7b] This was due to the low ratio of the distribution phase (α-phase) of the tetramer (26%), compared to the monomer and dimer, 39% and 36%, respectively. The increase in the molecular size led to retardation of the extravasation through the vascular endothelium. On the contrary, its lifetime (τ) of the disappearance phase (β-phase; 8.9 h) was shorter than the tightly bridged rHSA dimer with a sulfide bond (16.2 h); although the $\tau_{1/2}$ of the dimer is lower than the tetramer, there is a greater amount of dimer at 24 h than tetramer. The rHSA tetramer disappeared slowly after 12 h, and 10% remained at 24 h from the injection, which was almost the same amount observed in the monomer group. After 12 h, the weak disulfide bonds between the core and shell albumins may be cleaved to dissociate the monomer
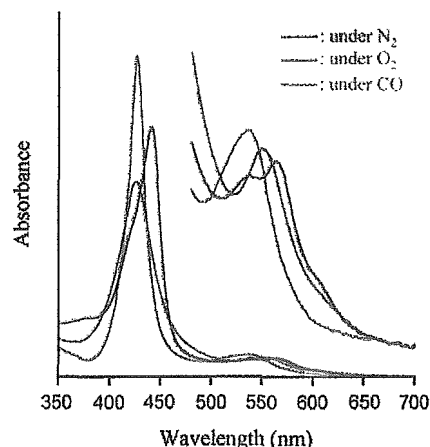

Figure 7. UV−vis absorption spectral changes of the rHSA−FeP tetramer in phosphate-buffered solution (pH 7.3) at various conditions (25 °C).

components and cleared from the bloodstream. Radioactivity of the trichloroacetic acid precipitates recovered up to 90% of the intensity, which means ^{125}I did not dissociate from the proteins. The tissue distributions of the rHSA tetramer were in the skin, liver, and spleen, and there were no differences to that of the rHSA monomer. Our albumin tetramer may become a unique vehicle which serves to sustain a high drug concentration particularly during the initial phase.

Albumin−Heme Clusters and Their O$_2$ Binding. Mixing the ethanolic FeP with an aqueous albumin cluster and removing the ethanol by ultrafiltration produced red-colored homogeneous albumin−heme cluster solutions. They were rather stable and stored for more than 1 year at 4 °C without any precipitation. From the quantitative assays of rHSA and FeP, the molar ratios of the FeP/rHSA were determined to be 24.2 and 31.6 for the trimer and tetramer, which are 3- and 4-fold molar excess amounts of the monomeric rHSA−FeP. We can conclude that a maximum of eight FePs were also incorporated into the rHSA unit. These albumin−heme clusters showed identical CD spectra and p*I* values (4.8) with the original rHSA trimer and tetramer, which implied that the FeP incorporation did not cause any structural changes in the albumin components.

The UV−vis absorption spectrum of the aqueous rHSA−FeP tetramer in an N$_2$ atmosphere showed the formation of a five-coordinate high-spin complex involving an axially bound 2-methylimidazolyl side-chain (λ_{max} = 444, 539, and 565 nm; Figure 7).[4b,8,13] After this solution was kept under a stream of O$_2$ for 5 min, the absorption spectra changed to that of a typical O$_2$−adduct complex (λ_{max} = 426 and 549 nm).[4b,8,13] This dioxygenation was reversibly observed and dependent on the O$_2$/N$_2$ pressure under physiological conditions (pH 7.3, 37 °C). After admitting the CO gas, the O$_2$−adduct complex immediately moved to the carbonyl low-spin complex (λ_{max} = 427 and 539 nm). The rHSA-FeP trimer also showed identical spectral changes under these conditions [rHSA-FeP trimer in N$_2$ (λ_{max} = 442, 539, and 564 nm), O$_2$ (λ_{max} = 423 and 547 nm), and CO atmosphere (λ_{max} = 426 and 534 nm)].
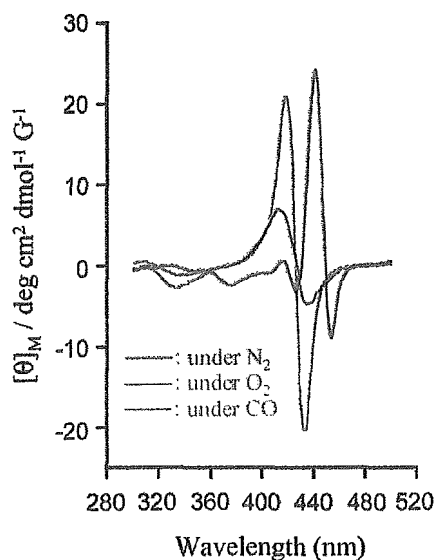
Figure 8. MCD spectral changes of the rHSA−FeP tetramer in phosphate-buffered solution (pH 7.3) at various conditions (25 °C).
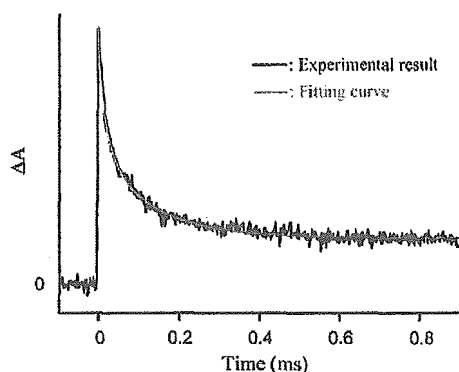

Figure 9. Absorption decay of O_2 rebinding to the rHSA−FeP cluster in phosphate-buffered solution (pH 7.3) after the laser flash photolysis at 25 °C. The kinetics was composed of three phases and relaxation curve was fitted by triple-exponentials.

MCD spectroscopy revealed the coordination structure of the FeP in the rHSA clusters. Under an N_2 atmosphere, the MCD of the rHSA-FeP tetramer resembled the well-characterized spectrum of a mono-imidazole ligated five-N-coordinate high-spin tetraphenylporphinatoiron(II) (Figure 8).[14] This observation indicates that the amino acid residue in the rHSA structure did not bind to the sixth position of FeP. The admission of O_2 gas changed the spectrum to an S-shaped A-term MCD in the Soret-band region, which shows the formation of an O_2−adduct complex.[14] The CO adduct is also low spin and exhibited a similar A-term MCD band with a high intensity.

The autoxidation reaction of the oxy state (λ_{max} = 549 nm) slowly occurred and the absorption intensity of 549 nm almost disappeared after 48 h, leading to the formation of the inactive Fe(III)P. The half-lives of the dioxygenated species ($\tau_{1/2}$) of the rHSA−FeP trimer and tetramer were both 7 h at 37 °C, which are almost the same as that of our previous results for the rHSA−FeP dimer ($\tau_{1/2}$ = 6 h).[7b]

O_2-Binding Kinetics and Equilibrium of Albumin−Heme Clusters. Flash photolysis experiments for the albumin−heme clusters were performed to determine the asso-

Table 2. O_2-Binding Parameters of rHSA-FeP Monomer, Dimer, and Clusters in Phosphate-Buffered Solution (pH 7.3) at 25 °C

	10^{-6} k_{on} $(M^{-1} s^{-1})$	10^{-6} K_{on} $(M^{-1} s^{-1})$	10^{-2} k_{off} (s^{-1})	10^{-2} K_{off} (s^{-1})	$P_{1/2}$ (Torr)[a]
rHSA-FeP[b]	46	7.3	9.8	1.6	13 (35)
rHSA-FeP dimer[c]	28	4.8	6.7	1.2	15 (38)
rHSA-FeP trimer	46	5.9	8.7	1.1	12 (38)
rHSA-FeP tetramer	53	13	11	2.7	12 (38)
Hb(T-state)α[d]	2.9		1.8		40
human RBC[e]					8 (27)

[a] At 37 °C in parenthesis. [b] From ref 8. [c] From ref 7b. [d] Hbα chain (monomer), aqueous pH 7.0–7.4, 20 °C, from ref 16. [e] From ref 17.
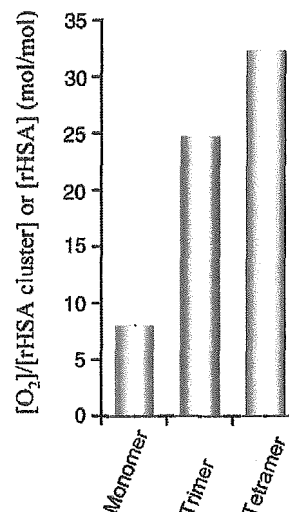

Figure 10. Molar ratio of the increased O_2 per rHSA cluster (mol/mol) after exposure of CO gas to rHSA−FeP cluster solutions (25 °C).

ciation and dissociation rate constants of O_2 (k_{on}, k_{off}). We have shown that the O_2 associations to FePs in the monomeric rHSA are affected by the molecular environments around the FeP site, for example, steric hindrance of the nearest amino acid residues.[4c] In the case of the albumin−heme clusters, there should be multiple kinetic parameters. Nevertheless, the O_2 binding profile to FeP demonstrated the same trends as the rHSA−FeP monomer. The absorption change accompanying the O_2 recombination clearly obeyed three-phases, which were fit by a triple-exponential kinetics (Figure 9). The fastest minor component (k_1) is related to a base dissociation reaction.[15] The linear relationship between the apparent rates k_2 and k_3 vs the [O_2] provided two association rate constants for the fast O_2 rebinding (k_{on}) and the slow O_2 rebinding (k'_{on}; Table 2). The k_{on} values are 4.1− 7.8-fold greater than k'_{on}, and the amplitude ratios of the fast and slow phases were approximately 1/1, which implied that half of the FeP molecules in the rHSA trimer and tetramer may locate in the slow sites for the O_2 association. The O_2-binding affinity ($P_{1/2}$) of the rHSA-FeP clusters were determined to be 38 Torr at 37 °C on the basis of the UV− vis. absorption spectral changes by O_2 titration with different [O_2].[4b,8,13] The obtained $P_{1/2}$ is close to that of the rHSA− FeP monomer and human RBC (Table 2).[8,16,17] The cluster formation did not alter the O_2-binding properties of rHSA− FeP.

O_2 Concentration in Albumin−Heme Cluster Solution.
The addition of small amounts of CO to the aqueous solutions of the dioxygenated rHSA−FeP clusters ([FeP] = 50 μM) in closed tubes dissociates the coordinated O_2, which immediately diffuses in the medium. In all cases, the O_2 concentrations increased 0.05 mM after the CO exposure. The UV−vis absorption spectra of the solutions changed to that of the carbonyl complex. The molar ratio of the chemically bound O_2 per albumin vehicle ([rHSA cluster] or [rHSA]) (mol/mol) showed that the albumin−heme clusters bind a large volume of O_2 relative to the monomer (Figure 10). The rHSA-FeP tetramer solution ([rHSA tetramer] = 0.75 mM, [heme] = 24 mM) could probably transport a 2.6-fold greater volume of O_2 compared to human blood ([heme] = 9.2 mM) while maintaining the colloid osmotic pressure on a physiological level.

Conclusions

The structurally defined albumin clusters prepared using a unique SH group of Cys-34 reported here provide the following characteristics.

(i) Essential properties of the rHSA units (the secondary/tertiary structure, surface net charges) were intact after the cluster formation. Our albumin clusters behave as a gigantic serum albumin.

(ii) The tetramer showed a longer half-life (5.5 h) in the bloodstream of rats compared to that of the monomer due to the low ratio of the α-phase (26%). However, it slowly disappeared after 12 h and was 10% of the basal value at 24 h after the injection.

(iii) The rHSA unit in the clusters can incorporate a maximum of eight FeP molecules, that is, the trimer and tetramer contain 24 and 32 active O_2-binding heme sites, which are 6- and 8-fold greater than that of the native tetrameric Hb, respectively. The obtained albumin−heme clusters become huge artificial hemoproteins with molecular weights of 235 and 313 kDa and can reversibly bind O_2 under physiological conditions.

(iv) The albumin−heme tetramer has the capability to transport a 4-fold larger volume of O_2 compared to the corresponding monomer when the albumin vehicle molar concentrations were identical. It implies that the albumin−heme clusters potentially become novel RBC substitutes having a 2.6-fold higher O_2 transporting ability than human blood.

This method of creating albumin clusters should lead to generating defined protein polymers and a new series of functional biomaterials. The preparations of the starburst rHSA dendrimer and linear string of rHSA pearls are now in progress.

References and Notes

(1) Peters, T., Jr. *All about albumin, biochemistry, genetics, and medical applications*; Academic Press: San Diego, CA, 1997; and reference therein.

(2) (a) Kragh-Hansen, U. *Pharmacol. Rev.* **1981**, *33*, 17−53. (b) Kragh-Hansen, U. *Danish Med. Bull.* **1990**, *37*, 57−84.

(3) Sheffield, W. P. *Curr. Drug Targets Cardiovasc. Haematol. Disord.* **2001**, *1*, 1−22.

(4) (a) Komatsu, T.; Hamamatsu, K.; Wu, J.; Tsuchida, E. *Bioconjugate Chem.* **1999**, *10*, 82−86. (b) Tsuchida, E.; Komatsu, T.; Matsukawa, Y.; Hamamatsu, K.; Wu, J. *Bioconjugate Chem.* **1999**, *10*, 797−802. (c) Komatsu, T.; Matsukawa, Y.; Tsuchida, E. *Bioconjugate Chem.* **2000**, *11*, 772−776.

(5) Tsuchida, E.; Komatsu, T.; Matsukawa, Y.; Nakagawa, A.; Sakai, H.; Kobayashi, K.; Suematsu, M. *J. Biomed. Mater. Res.* **2003**, *64A*, 257−261.

(6) Carter, D. C.; Ho, J. X. *Adv. Protein Chem.* **1994**, *45*, 153−203.

(7) (a) Komatsu, T.; Hamamatsu, K.; Tsuchida, E. *Macromolecules* **1999**, *32*, 8388−8391. (b) Komatsu, T.; Oguro, Y.; Teramura, Y.; Takeoka, S.; Okai, J.; Anraku, M.; Otagiri, M.; Tsuchida, E. *Biochim. Biophys. Acta* **2004**, *1675*, 21−31.

(8) Komatsu, T.; Matsukawa, Y.; Tsuchida, E. *Bioconjugate Chem.* **2002**, *13*, 397−402.

(9) Doumas, B. T.; Watson, W. A.; Biggs, H. G. *Clin. Chim. Acta* **1971**, *31*, 87−96.

(10) Grassetti, D. R.; Murray, J. F., Jr. *Arch. Biochem. Biophys.* **1967**, *119*, 41−49.

(11) Pedersen, A. O.; Jacobsen, J. *Eur. J. Biochem.* **1980**, *106*, 291−295.

(12) Watanabe, H.; Yamasaki, K.; Kragh-Hansen, U.; Tanase, S.; Harada, K.; Suenaga, A.; Otagiri, M. *Pharm. Res.* **2001**, *18*, 1775−1781.

(13) Collman, J. P.; Brauman, J. I.; Iverson, B. L.; Sessler, J. L.; Morris, R. M.; Gibson, Q. H. *J. Am. Chem. Soc.* **1983**, *105*, 3052−3064.

(14) (a) Collman, J. P.; Brauman, J. I.; Doxsee, K. M.; Halbert, T. R.; Bunnenberg, E.; Linder, R. E.; LaMar, G. N.; Guadio, J. D.; Lang, G.; Spartalian, K. *J. Am. Chem. Soc.* **1980**, *102*, 4182−4192. (b) Collman, J. P.; Basolo, F.; Bunnenberg, E.; Collins, T. C.; Dawson, J. H.; Ellis, P. E., Jr.; Marrocco, M. L.; Moscowitz, A.; Sessler, J. L.; Szymanski, T. *J. Am. Chem. Soc.* **1981**, *103*, 5636−5648.

(15) Geibel, J.; Cannon, J.; Campbell, D.; Traylor, T. G. *J. Am. Chem. Soc.* **1978**, *100*, 3575−3585.

(16) Sawicki, C. A.; Gibson, Q. H. *J. Biol. Chem. Soc.* **1977**, *252*, 7538−7547.

(17) Severinghous, J. W. *J. Appl. Physiol.* **1966**, *21*, 1108−1116.

BM050454U

Human Serum Albumin Hybrid Incorporating Tailed Porphyrinatoiron(II) in the α,α,α,β-Conformer as an O2-Binding Site

Akito Nakagawa, Teruyuki Komatsu,* Makoto Iizuka, and Eishun Tsuchida*

Advanced Research Institute for Science and Engineering, Waseda University, 3-4-1 Okubo, Shinjuku-ku, Tokyo 169-8555 Japan. Received June 1, 2005; Revised Manuscript Received October 30, 2005

We have found that recombinant human serum albumin (HSA) incorporating tailed porphyrinatoiron(II) in the α,α,α,β-conformer can reversibly bind and release O2 under physiological conditions (pH 7.3, 37 °C) like hemoglobin and myoglobin. β-2-Methylimidazolyl-tailed porphyrinatoirons (6a, 6b) are synthesized via four steps from the atropisomers of tetrakis(o-aminophenyl)porphyrin. The stereochemistry of the α,α,α,β-conformer has been determined by NMR spectroscopy. 6a and 6b form stable O2-adduct complexes in toluene solution at room temperature. The association rate constants of O2 are 3.1- and 1.9-fold lower than those of the corresponding α,α,α,α-conformers (1a, 1b), indicating that the three substituents (cyclohexanamide or pivalamide groups) are close to each other on the porphyrin platform and construct a narrow encumbrance around the O2-coordination site. Although 6a and 6b are incorporated into the hydrophobic domains of HSA to produce the albumin—heme hybrid, only HSA-6a can bind O2 in aqueous medium. The cyclohexanamide fences are necessary for the tailed porphyrinatoiron to form a stable O2-adduct complex under physiological conditions. The O2-binding affinity ($P_{1/2}$) of HSA-6a is 45 Torr (37 °C), and the O2 transporting efficiency between lungs and muscle tissues in the human body is estimated to be identical to that of human red blood cells. The HSA-6a solution will become one of the most promising materials for red blood cell substitutes, which can be manufactured on an industrial scale.

INTRODUCTION

To reproduce the O2-binding ability of hemoglobin (Hb) and myoglobin (Mb), numerous numbers of model hemes have been synthesized over the past decades (1). These continuous approaches, aimed at understanding the precise mechanism of the O2-binding reaction, have been mostly accomplished in organic solvents, and tetrakis(phenyl)porphyrin (TPP) was widely used as a molecular scaffold. We have also synthesized tetrakis-{α,α,α,α-o-(1-methylcyclohexanamido)phenyl}porphinatoiron-(II) bearing a covalently linked proximal imidazole (1a, Figure 1)[1] that forms a stable O2-adduct complex in toluene solution at ambient temperature (2). The four cyclohexanamide fences on the distal-side (α-side) of the porphyrin plane are bulky enough to prevent μ-oxo dimer formation, and the 2-methylimidazolyl arm intramolecularly coordinated to the Fe²⁺ center from the proximal-side (β-side) modulates the O2-binding affinity.

Some substantial efforts have been directed to prepare an artificial O2 carrier involving a synthetic heme under physiological conditions (pH 7.3, 37 °C), which may become a red blood cell substitute (1a, 3). We have successfully incorporated 1a into the hydrophobic domains of recombinant human serum albumin (HSA) and found that the albumin—heme hybrid (HSA—1a) could reversibly absorb O2 in aqueous medium (1a, 2, 4). This red-colored albumin solution showed a long shelf life of over two years without precipitation. More recently,
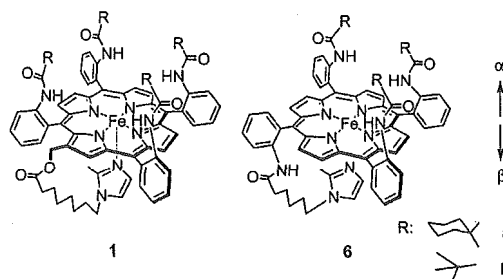
¹ Abbreviations: 1a: 2-[8-{N-(2-methyl-1-imidazolyl)octanoyloxy]-methyl]-5,10,15,20-tetrakis{(α,α,α,α-o-(1-methylcyclohexanamido)-phenyl}porphinatoiron; 1b: 2-[8-{N-(2-methyl-1-imidazolyl)octanoyl oxymethyl]-5,10,15,20-tetrakis{α,α,α,α-o-(pivalamido)phenyl}porphinatoiron; 6a: 5,10,15-Tris {α,α,α-o-(1-methylcyclohexanamido)-phenyl}-20-mono[β-o-[6-{N-(2-methyl-1-imidazolyl)}hexanamido]phenyl]-porphinatoiron; 6b: 5,10,15-Tris(α,α,α-o-(pivalamido)phenyl)-20-mono[β-o-[6-{N-(2-methyl-1-imidazolyl)}hexyramido]phenyl]-porphinatoiron.

Figure 1. Structures of porphyrinatoiron derivatives in the α,α,α,α-conformer and α,α,α,β-conformer (tailed porphyrinatoiron).

exchange transfusion experiments with HSA—1a into anesthetized rats demonstrated that it effectively rescitates the hemorrhagic shock state and transports O2 to the muscle tissues (5). We are now developing this albumin—heme hybrid as an entirely synthetic red blood cell substitute that can be extensively used in a variety of medical situations (6).
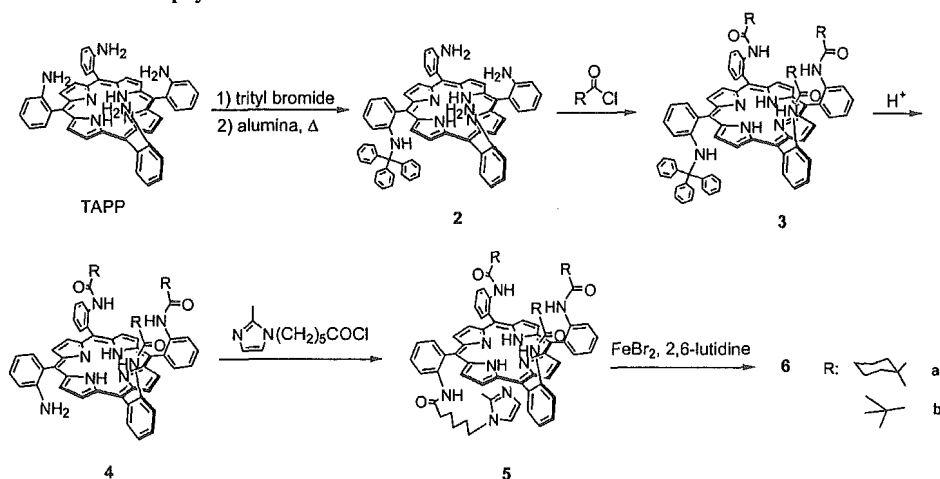
The only disadvantage of this synthetic heme 1a is that a great deal of labor is required to make the α,α,α,α (α⁴)-conformer and to introduce the imidazolylalkyl arm at the porphyrin periphery via the Vilsmeier reaction (2). The starting material, tetrakis(α,α,α,α-o-aminophenyl)porphyrin (TAPP), is in a statistical mixture of the four possible atrop isomers (α,α,α,α, α,α,α,β, α,β,α,β, α,α,β,β; the ratio is 1:4:2:1), and the variable α⁴-conformer used to be isolated by Lindsey's procedure with a silica gel column separation (7). The number of total steps for the synthesis of 1a is, therefore, eight from TAPP.

In this study, we first incorporated a "tailed porphyrinatoiron" with the α³β-conformer as an O2-binding site of the albumin—heme. A series of tailed porphyrins as the model compound of Hb and Mb were synthesized by Collman and co-worker (8). There are two advantages of the tailed porphyrin: (i) the statistical content of the α³β-conformer of TAPP is maximum

Scheme 1. Synthesis of Tailed Porphyrinatoirons

(50%), and (ii) there is no need to modify the porphyrin ring because the proximal base is attached to the fourth β-o-NH$_2$ group of the phenyl ring. This convenient synthetic procedure is a great advantage for the industrial scale-up of the manufacturing of the albumin—heme solution. However, we were not certain of the stability of the O$_2$-adduct complex of the tailed porphyrinatoiron(II) in an aqueous medium. It has been postulated that the four substituents were essential for preventing an unfavorable proton-driven oxidation of the central ferrous ion of the Fe^{2+}TPP derivatives in water (*1a, 3*).

First, we describe the synthesis and stereochemistry of the 2-methylimidazole-tailed porphyrinatoirons (**6a, 6b**) and compare their O$_2$-binding properties in toluene solution. The effects of the substituents on the O$_2$-binding parameters are discussed. Furthermore, the O$_2$-binding property of the albumin—heme hybrid including the tailed porphyrinatiron(II) **6a** has been characterized under physiological conditions. The 5 wt % albumin—heme solution involving the easily prepared **6a** could be the most promising artificial O$_2$ carrier suitable for mass production.

EXPERIMENTAL SECTION

Synthesis of Tailed Porphyrinatoirons. Experimental details of the synthesis and spectra (^{1}H NMR, IR, UV—Vis, HR-MS) are supplied as Supporting Information.

Reduction of Ferric Complex to Ferrous Complex in Toluene. Reduction to the porphyrinatoiron(II) was carried out using toluene-aq Na$_2$S$_2$O$_4$ in a heterogeneous two-phase system under an N$_2$ atmosphere as previously reported (*9*). After separation of the two phases, the organic layer containing the ferrous complex was transferred to a 1-cm quartz cuvette under an N$_2$ atmosphere. The UV—Vis absorption spectra were recorded by a JASCO V-570 spectrophotometer.

Preparation of Albumin—Heme Hybrid. The HSA (Albrec, 25 wt %) was obtained from the NIPRO Corp. (Osaka). Aqueous ascorbic acid (15 mM, 20 μL) was added to an ethanol solution of the porphyrinatoiron(III) derivative (37.5 μM, 4 mL) under CO. After complete reduction of the central ferric ion, the UV—Vis absorption spectrum showed the formation of the six-coordinated carbonyl complex. This ethanol solution was slowly injected into the phosphate buffered solution (pH 7.3, 8 mL) of HSA (9.38 μM) through a Teflon tube under a pressure of CO stream. The mixture was dialyzed using a cellulose membrane against phosphate buffer (pH 7.3) for 2 and 15 h at 4 °C. The ethanol concentration should be reduced to less than 100 ppm. Finally, the total volume was adjusted to 15 mL, thus producing the carbonyl albumin—heme solution (heme/HSA = 4 (mol/

mol), [Fe]: 20 μM). The water was deionized using an ADVANTEC GS-200 system.

O$_2$-Coordination Equilibria and Kinetics. The O$_2$-binding affinity ($P_{1/2}$) of the porphyrinaoitron(II) in organic solvents or their albumin—hemes in aqueous solution were determined by the spectral changes at various partial pressures of O$_2$ in previous reports (*2, 10*). The heme concentrations of 20 μM were normally used for the UV—Vis absorption spectroscopy. The spectra were recorded within the range of 350—700 nm. The O$_2$-association and -dissociation rate constants (k_{on}, k_{off}) were measured by a competitive rebinding technique (*11, 12*) using a Unisoku TSP-1000WK-WIN time-resolved spectrophotometer with a Spectron Laser system SL803G-10 Q-switched Nd:YAG laser, which generated a 532 nm pulse of 6-ns duration (10 Hz).

Magnetic Circular Dichroism (MCD). The MCD for the phosphate buffered solutions (pH 7.3) of HSA—**6a** (20 μM) under N$_2$, O$_2$, and CO atmospheres were measured using a JASCO J-820 circular dichrometer fitted with a 1.5 T electromagnet at 25 °C. The accumulation times were normally five, and each spectra were subtracted by ones without the electromagnetic as a baseline.

RESULTS AND DISCUSSION

Synthesis of Tailed Porphyrinatoiron. The tailed porphyrinatoirons, **6a** and **6b**, can be synthesized via four reaction steps from TAPP with 6-{N-(2-methyl-1-imidazolyl}hexanoic acid (Scheme 1), and their structures were determined by IR, UV, mass and NMR (^{1}H NMR, H—H COSY, Nuclear Overhauser effect (NOE) experiment) spectroscopies. First, TAPP was monotritylated using tritylbromide at room temperature. Statistically, six atrop isomers of the monotritylated compound are formed. Collman and co-workers reported the superior synthesis of tris(α,α,α-aminopheny)-mono(β-tritylaminophenyl)porphyrin (**2**) using the alumina absorption technique in the dark (*13*). We isolated two major components from the reaction mixture according to the procedure with the R_f values (chloroform/ethyl acetate = 1:1 (v:v)) of 0.75 (compound A) and 0.90 (compound B). The coupling reaction of compound A with pivaloyl chloride gave a single product, tris(pivalamido)phenyl-monotritylphenyl-porphyrin (compound **A1**). On the other hand, the same coupling reaction of compound B provided two products (compounds **B1** and **B2**) with R_f values (chloroform/ethyl acetate = 2:1 (v/v)) of 0.68 and 0.62, respectively. The mass spectra of the above three compounds exactly demonstrated the same value (calcd. for C$_{78}$H$_{73}$N$_8$O$_3$: 1169.5806), indicating that **A1**, **B1**, and **B2** are atrop isomers. In ^{1}H NMR spectra of **A1** and **B1**, the peaks derived from the CH$_3$ protons in the pivalamide groups were

Scheme 2. Atropisomers of 2 and Their Pivalamide Derivatives
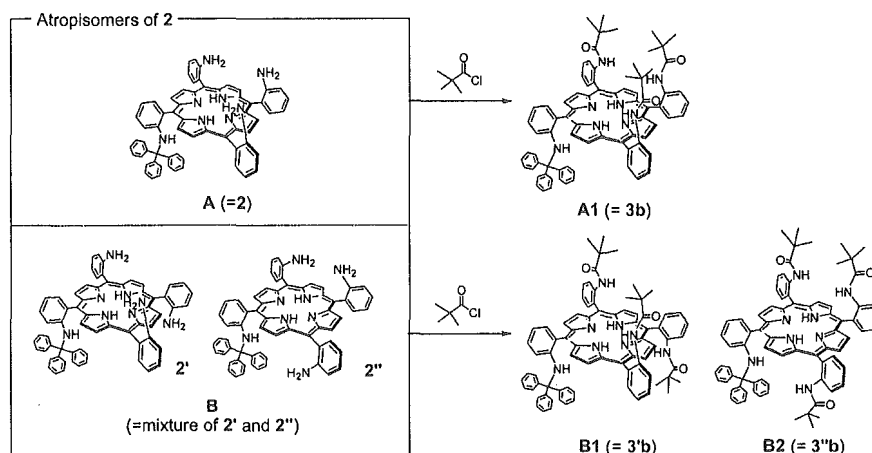
clearly separated into two peaks, and the patterns resembled those of the other $\alpha^3\beta$-structured TAPP derivatives (*14*, *15*) (see Figures ESI1—ESI3, Supporting Information). The differences in the chemical shift between the two peaks were 0.12 (**A1**) and 0.15 (**B1**) ppm, respectively. The CH₃ peaks of **B2** were also splited, but the peak separation was rather small, 0.01 ppm.

To clarify the stereochemistry of these atrop isomers and the geometry of the substituents, we employed the NOE differential spectra (*16*) (see Figures ESI1—ESI3, Supporting Information). In porphyrin **A1**, three pivalamide groups are directed toward the same side and a trityl group is directed only toward the other side, which means **A1** is the target compound **3b**. In **B1**, one of the pivalamide groups is in the same plane with the trityl group, but they do not interact with each other. This result suggests the formation of the $\alpha,\beta,\alpha,\beta$-conformer **3'b**. In **B2**, at least one pivalamide group is on the same side with the trityl group. In this case, there are four atrop isomers expected, but we concluded **B2** would be the $\alpha,\alpha,\beta,\beta$-structure (**3''b**) because the parent compound **B** was less polar than compound **A** in the $\alpha^3\beta$-conformer. In summary (Scheme 2), (i) compound **A** is porphyrin **2** in the $\alpha^3\beta$-conformer, (ii) compound **B** is a mixture of **2'** ($\alpha,\beta,\alpha,\beta$-conformer) and **2''** ($\alpha,\alpha,\beta,\beta$-conformer). Our attempts to perform the same NOE experiment on **3a** unfortunately failed because it was difficult to saturate only the peak of the 1-methyl group at the bottom of cyclohexane ring. The coupling reaction of **2** with 1-methylcyclohexanoyl chloride gave the desired **3a** (yield: 53%).

After detritylation under acidic conditions, 6-(2-methylimidazole-1-yl)hexanoic acid chloride was reacted with the β-o-NH₂ group of **4**. Iron insertions of these free base porphyrins were performed with an excess of FeBr₂ with 2,6-lutidine as the base. The total yields of **6a** and **6b** were 15 and 10% from the atrop-isomeric mixture of TAPP. All these compounds are now available in gram quantities.

During the synthesis of the tailed porphyrinatoiron, we are always careful to prevent the atrop isomerizations of the products. The bulky pivalamide or 1-methylcyclohexanamide substituted phenyl rings did not rotate with respect to the porphyrin plane by the ambient light and heating even at 100 °C in toluene for 2 h (*8*). However, the same heating of the detritylated porphyrin **4** afforded two components, the unchanged original **4** and the new one with a lower R_f value. They both showed identical molecular weights. The newly appearing compound is suspected to be the porphyrin **4'** in the α^4-conformer. Tritylation of **4'** again by the same procedure for TAPP with tritylbromide did not proceed at all due to the steric hindrance of the fence groups next to the NH₂ group.

Table 1. Absorption Maxima (λ_{max}) of Tailed Porphyrinatoiron(II) in Toluene

| | λ_{max} | | |
	under N₂	under O₂	under CO
6a	438, 535, 558	426, 550	424, 535
6b	435, 535, 555	422, 546	421, 534
1a	441, 539, 558	424, 552	425, 534
1b[a]	439, 535, 561	422, 550	422, 534

[a] Reference 10b.

Table 2. O₂-Binding Parameters of Tailed Porphyrinatoiron(II) in Toluene at 25°C

	k_{on} (M⁻¹ s⁻¹)	k_{off} (s⁻¹)	$P_{1/2}$ (Torr)
6a	5.8×10^7	5.1×10^4	67
6b	8.6×10^7	5.6×10^4	50
1a[a]	1.8×10^8	4.7×10^4	20
1b[a]	1.6×10^8	7.9×10^4	38

[a] Reference 2.

O₂-Binding Properties of Tailed Porphyrinatoiron(II) in Toluene Solution. UV—Vis absorption spectra of ferrous **6a** and **6b** in toluene solution under an N₂ atmosphere were very similar to those of the five-N-coordinate complexes of **1a** and **1b** (Table 1). This indicates that **6a** and **6b** are also five-N-coordinate high-spin Fe²⁺ complex with an intramolecularly coordinated imidazole tail. Upon bubbling of O₂ gas into these solutions, the absorption spectra immediately changed to that of the well-characterized O₂ adduct complex of the Fe²⁺TPP derivative. After passing the CO gas, the spectral pattern was converted to the typical carbonyl complex. There is no significant difference in the λ_{max} values of **6a**, **6b**, **1a**, and **1b** within 6 nm.

The binding affinities ($P_{1/2}$), association and dissociation rate constants (k_{on}, k_{off}) of O₂ to the tailed porphyrinatoiron(II)s, **6a** and **6b**, were determined (Table 2). We thought that the reduction of the fence numbers on the porphyrin ring plane from four to three unfastens the steric hindrance around the O₂-coordination site and enhanced the association rate constant of O₂. It is generally recognized that the k_{on} value increases with the relaxing distal steric encumbrance (*1*, *11*, *12*, *15*). However, the reverse was the case. In contrast to our assumption, the k_{on} values of the tailed porphyrinatoirons, **6a** and **6b**, were 3.1- and 1.9-fold lower than the corresponding α^4-conformers (**1a** and **1b**), respectively, while their k_{off} values were nearly the same. This result suggests that the steric hindrances for the O₂ association to **6a** and **6b** are greater than those of **1a** and **1b**. Most probably, three fences on the amide bonds in the $\alpha^3\beta$-
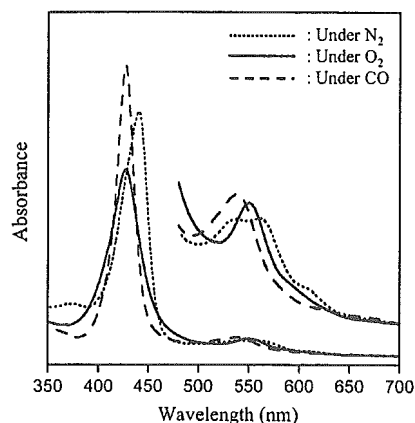
Figure 2. UV—Vis absorption spectral change of HSA—6a hybrid in phosphate buffered solution (pH 7.3).

Table 3. Absorption Maxima (λ_{max}) of HSA—Tailed Porphinatoiron (II) Hybrid in Phosphate Buffered Solution (pH 7.3)

	λ_{max}		
	under N_2	under O_2	under CO
HSA-6a	440, 536, 559	427, 550	427, 539
HSA-6b	—	—	424, 537
HSA-1a[a]	445, 543, 567	428, 555	429, 545
HSA-1b[a]	443, 542, 567	426, 552	427, 539

[a] Reference 2.

conformer can easily move on the porphyrin platform compared to the crowded four fences of the α^4-conformer. These flexible geometries of the substituents, if anything, narrowed the encumbrance around the O_2-coordination site relative to the α^4 arrangement.

O_2-Binding Properties of HSA-Tailed Porphyrinatoiron in Aqueous Medium. The tailed porphyrinatoirons, 6a and 6b, in the $\alpha^3\beta$-conformer could be incorporated into hydrophobic domains of HSA, providing the corresponding albumin—heme hybrids. Their maximum binding numbers to HSA were determined to be approximately 8 (mol/mol), which is identical to those of 1a and 1b (2, 10a). It is known that HSA binds porphyrin derivatives and their binding sites largely depend on the chemical structures, hydrophobicity, and electrostaticity. Crystal structure analysis of HSA complexed with natural Fe^{3+} protoporphyrin IX, namely, hemin, revealed that hemin is accommodated into subdomain IB of HSA (17). On the other hand, hematoporphyrin is incorporated into subdomain IIIA (18), and tetrakis(p-sulfonatophenyl)porphyrin binds to subdomain IIA or IIIA (19). On the basis of the competitive binding inhibition, we supposed that the some of the binding sites of 1a are subdomains IB, IIA, and IIIB (10a). Attempts to crystallize HSA—6a hybrid are now underway, but the porphyrin 6a dissociated from albumin during the crystallization process due to the relatively low binding constants of 6a to HSA (10^6—10^4 M^{-1}) and coexistence of poly(ethylene glycol) in the media. We suspect that the binding sites of 6a and 6b are the same places of 1a. The isoelectric point ($pI = 4.8$) and circular dichroism spectral patterns of HSA—6a and HSA—6b were similar to those of HSA itself, indicating that the surface and conformation of albumin were unaltered after bindings of the tailed porphyrinatoirons.

UV—Vis absorption spectra of the freshly prepared ferrous HSA—6a showed λ_{max} values at 424 and 537 nm (Figure 2, Table 3). This spectrum was almost identical to that of the CO coordinated low-spin 6a in toluene solution, implying that the incorporated tailed porphyrinatoiron(II) is still the CO adduct complex in HSA. Light irradiation to this aqueous HSA—6a using a 500-W halogen lamp under an O_2 atmosphere leads to
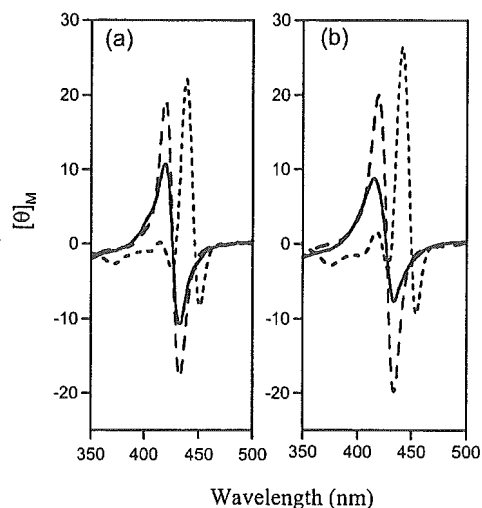

Figure 3. MCD spectral changes of (a) HSA—6a and (b) HSA—1a hybrids in phosphate buffered solution (pH 7.3). Solid line: under O_2; dotted line: under N_2; dashed line: under CO.

Table 4. O_2-Binding Parameters of HSA—Tailed Porphinatoiron (II) Hybrid in Phosphate Buffered Solution (pH 7.3) at 25°C

	k_{on} (M^{-1} s^{-1})		k_{off} (s^{-1})		
	fast	slow	fast	slow	$P_{1/2}$ (Torr)[a]
HSA—6a	2.9×10^7	4.4×10^6	1.1×10^3	1.6×10^2	22 (45)[b]
HSA—1a[c]	4.6×10^7	7.3×10^6	9.8×10^2	1.6×10^2	13 (35)[b]

[a] $P_{1/2} = (k_{on}/k_{off})^{-1}$. [b] At 37 °C in parentheses. [c] Reference 2.

CO dissociation, giving a typical spectral pattern of the O_2 adduct complex. Upon exposure of the dioxygenated HSA—6a to N_2, the absorption spectrum changed to that of the five-N-coordinated ferrous complex with an intramolecularly coordinated axial imidazole. This O_2 binding and releasing were found to be reversible.

In contrast, the ferrous HSA—6b was irreversibly oxidized during the CO dissociation process under an O_2 atmosphere. We concluded that the bulky and hydrophobic substituent like the 1-methylcyclohexanamide fences are necessary for the tailed porphyrinatoiron(II) in the $\alpha^3\beta$-conformer to form a stable O_2 adduct complex under physiological conditions (pH 7.3, 37 °C).

The magnetic circular dichloisim (MCD) spectra of HSA—6a showed almost the same pattern as those of HSA—1b (Figure 3) (20). Under an N_2 atmosphere, the MCD spectrum of HSA—6a showed the formation of the five-coordinate ferrous high-spin complex of 6a with the intramolecular coordinated proximal imidazole. This result showed no ligation of the amino acid residues of the protein, e.g., histidine, tyrosine, cysteine, to the sixth coordination site of the heme. The bulky fences on the porphyrin plane could prevent access of the neighboring peptide residues to the sixth coordination site of 6a. Upon exposure of this solution to O_2, the spectrum immediately changed and showed an S-shaped A-term MCD in the Soret region, which indicates a transformation to the ferrous low-spin complex (8, 21). The CO adduct complex of HSA—6a also exhibited a similar A-term MCD band in the same region with a much stronger intensity. The wavelength where the value of $[\theta]_M$ is zero for the O_2 and CO adduct complex coincided well with the absorption maxima in their corresponding UV—Vis spectra.

The $P_{1/2}$ of the HSA—6a was determined by measuring the UV—Vis absorption spectral changes during the O_2 titration. The laser flash photolysis experiments provided the k_{on} and k_{off} values of the O_2 binding to HSA—6a (Table 4). The absorption decays accompanying the O_2 recombination were composed of two-phases of the first-order kinetics. The curve was fitted by
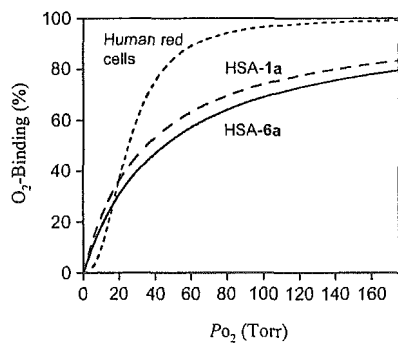
Figure 4. O_2-binding equilibrium curve of HSA−6a under physiological conditions (pH 7.3, 37 °C).

a double exponential equation, which was assigned to the fast and slow rebindings [k_{on}(fast) and k_{on}(slow)] of O_2. The k_{on}(fast) values were 7 times greater than k_{on}(slow), and the concentration ratio of the fast and slow reactions was 2:1. This is presumably because the O_2 association to **6a** in HSA is influenced by the molecular microenvironment in the hydrophobic domains (steric hindrance of the amino acid residue and difference in polarity). This behavior was similarly observed in HSA−**1a** and HSA−**1b** (*2, 22*). The k_{on} values of HSA−**6a** are again 1.6−1.7-fold lower than those of HSA−**1a** in aqueous medium as observed in toluene solution. This is also caused by the narrow encumbrance on the porphyrin ring plane constructed by the three 1-methlcyclohexanamide fences of **6a**.

The HSA−**6a** did not show a cooperative O_2-binding profile like Hb; the Hill coefficient was 1.0 (Figure 4). Although the O_2-binding affinity of HSA−**6a** at 37 °C is relatively low ($P_{1/2}$ value (45 Torr) is high) compared to those of HSA−**1a** (35 Torr) and human red blood cells (28 Torr), the O_2-transporting efficiency of HSA−**6a** between the lungs (Po_2: 110 Torr) and muscle tissues (Po_2: 40 Torr) is estimated to be 22%, which is identical to human red blood cells and HSA−**1a**.

CONCLUSIONS

Tailed porphyrinatoirons have been first employed as an O_2-binding site of the synthetic hemoprotein, albumin−heme. **6a** and **6b** with a β-o-(2-methylimidazolyl)hexyramide tail have been easily synthesized via four steps from the TAPP scaffold compared to the eight steps of **1a**. The stereochemistry of the $\alpha^3\beta$-conformer was confirmed by NOE experiments. The association rates of O_2 were slower than for the corresponding α^4-conformers, which indicates that three substituents are close to the porphyrin platform and narrowed the encumbrance space around the O_2-coordination site. As an active site for the albumin−heme hybrid, **6a** was effective, but **6b** was rapidly oxidized. It can be concluded that bulky and hydrophobic substituents like the 1-methylcyclohexanamide fences are necessary for obtaining a stable O_2 adduct complex. The O_2 transporting ability of the HSA−**6a** was almost the same as human red blood cells. Currently, since HSA is manufactured on a large scale by yeast expression (*23*), the 5 wt % albumin−heme solution involving **6a** as O_2 binding site is the most promising material as a red blood cell substitute and O_2-carrying therapeutic reagent, which would be mass produced on an industrial scale.

ACKNOWLEDGMENT

Supporting Information Available: Synthetic procedure of the tailed porphyrinatoirons (**6a, 6b**); ^{1}H NMR and NOE differential spectra of compounds **A1**, **B1**, and **B2**. These materials are available free of charge via the Internet at http://pubs.acs.org.

LITERATURE CITED

(1) (a) Collman, J. P., Boulatov, R., Sunderland, C. J., and Fu, L. (2004) Functional analogues of cytochrome c oxidase, myoglobin, and hemoglobin. *Chem. Rev. 104*, 561−588. (b) Momenteau, M., and Reed, C. A. (1994) Synthetic heme-dioxygen complexes. *Chem. Rev. 94*, 659−698 and references therein.

(2) Komatsu, T., Matsukawa, Y., and Tsuchida E. (2002) Effect of heme structure on O_2-binding properties of human serum albumin-heme hybrids: Intramolecular histidine coordination provides a stable O_2-adduct complex. *Bioconjugate Chem. 13*, 397−402.

(3) Komatsu, T., Moritake, M., Nakagawa, A., and Tsuchida, E. (2002) Self-organized lipid-porphyrin bilayer membranes in vesicular form: Nanostructure, photophysical properties and dioxygen coordination. *Chem. Eur. J. 8*, 5469−5480.

(4) Komatsu, T., Oguro, Y., Teramura, Y., Takeoka, S., Okai, J., Anraku, M., Otagiri, M., and Tsuchida, E. (2004) Physicochemical characterization of cross-linked human serum albumin dimer and its synthetic heme hybrid as an oxygen carrier. *Biochim. Biophys. Acta 1675*, 21−31.

(5) (a) Huang, Y., Komatsu, T., Yamamoto, H., Horinouchi, H., Kobayashi, K., and Tsuchida, E. (2004) Safety evaluation of an artificial O_2 carrier as a red blood cell substitute by blood biochemical tests and histopathology observations, *ASAIO J. 50*, 525−529. (b) Komatsu, T., Huang, Y., Yamamoto, H., Horinouchi, H., Kobayashi, K., and Tsuchida, E. (2004) Exchange transfusion with synthetic oxygen-carrying plasma protein "albumin-heme" into an acute anemia rat model after seventy-percent hemodilution. *J. Biomed. Mater. Res. 71A*, 644−651. (c) Huang, Y., Komatsu, T., Yamamoto, H., Horinouchi, H., Kobayashi, K., and Tsuchida, E. (2004) Exchange transfusion with entirely synthetic red-cell substitute albumin-heme into rats: physiological responses and blood biochemical tests. *J. Biomed. Mater. Res. 71A*, 63−69.

(6) Kobayashi, K., Komatsu, T., Iwamaru, A., Matsukawa, Y., Horinouchi, H., Watanabe, M., and Tsuchida, E. (2002) Oxygenation of hypoxic region in solid tumor by administration of human serum albumin incorporating synthetic hemes. *J. Biomed. Mater. Res. 64A*, 48−51.

(7) Lindsey, J. (1980) Increased yield of a desired isomer by equilibriums displacement on binding to silica gel, applied to mesotetrakis(o-aminophenyl)porphyrin. *J. Org. Chem. 45*, 5215−5215.

(8) Collman, J. P., Brauman, J. I., Doxsee, K. M., Halbert, T. R., Bunnenberg, E., Linder, R. E., LaMar, G. N., Gaudio, J. D., Lang, G., and Spartalian, K. (1980) Synthesis and characterization of "tailed picket fence" porphyrins. *J. Am. Chem. Soc. 102*, 4182−4192.

(9) Tsuchida, E., Hasegawa, E., Komatsu, T., Nakata, T., Nakao, K., and Nishide, H. (1991) Synthesis and coordination behaviors of new double-sided porphyrinatoiron(II) complexes: effect of the pocket size for imidazole on dioxygen binding. *Bull. Chem. Soc. Jpn. 64*, 888−894.

(10) (a) Komatsu, T., Hamamatsu, K., Wu, J., and Tsuchida, E. (1999) Physicochemical properties and O_2-coordination structure of human serum albumin incorporating tetrakis-(o-pivalamido)phenylporphyrinatoiron(II) derivatives. *Bioconjugate Chem. 10*, 82−86. (b) Tsuchida, E., Komatsu, T., Kumamoto, S., Ando, K., and Nishide, H. (1995) Synthesis and O_2-binding properties of tetraphenylporphyrinatoiron(II) derivatives bearing a proximal imidazole covalently bound at the β-pyrrolic position. *J. Chem. Soc., Perkin Trans. 2.* 747−753.

(11) Collman, J. P., Brauman, J. I., Iverson, B. L., Sessler, J. L., Morris, R. M., and Gibson, Q. H. (1983) O_2 and CO binding to iron(II) porphyrins: A comparison of the "picket fence" and "pocket" porphyrins. *J. Am. Chem. Soc. 105*, 3052−3064.

(12) Traylor, T. G., Tsuchiya, S., Campbell, D., Mitchell, M., Stynes, D., and Koga, N. (1985) Anthracene heme cyclophanes. Steric Effects in CO, O_2 and RNC Binding. *J. Am. Chem. Soc. 107*, 604−614.

(13) Collman, J. P., Broring, M., Fu, L., Rapta, M., Schwenninger, R., and Straumanis, A. (1998) Novel protecting strategy for the synthesis of porphyrins with different distal and proximal superstructures. *J. Org. Chem. 63*, 8082−8083.

(14) Inaba, Y., and Kobuke, Y. (2004) Synthesis of a complementary dimer from mono(imidazolyl)-substituted cobalt(II) porphyrin as a new artificial T-form hemoglobin. *Tetrahedron 60*, 3097−3107.

(15) Wuenschell, G. E., Tetreau, C., Lavalette, D., and Reed, C. A. (1992) Hydrogen-bonded oxyhemoglobin models with substituted picket-fence porphyrins: the model compound equivalent of site-directed mutagenesis. *J. Am. Chem. Soc. 114*, 3346−3355.

(16) Collman, J. P., Sunderland, C. J., and Boulatov, R. (2002) Biomimetic studies of terminal oxidases: trisimidazole picket metalloporphyrins. *Inorg. Chem. 41*, 2282−2291.

(17) Zunszain, P. A., Ghuman, J., Komatsu, T., Tsuchida, E., and Curry, S. (2003) Crystal structural analysis of human serum albumin complexes with hemin and fatty acid, *BMC Struct. Biol. 3*, 6.

(18) Cohen, S., and Margalit, R. (1990) Binding of porphyrin to human serum albumin, structure−activity relationship. *Biochem. J. 270*, 325−330.

(19) Andrade, S. M., and Costa, S. M. B. (2002) Spectroscopic studies on the interaction of a water soluble porphyrin and two drug carrier proteins. *Biophys. J. 82*, 1607−1619.

(20) Tsuchida, E., Nakagawa, A., and Komatsu, T. (2003) Coordination structure of active site in synthetic hemoprotein (albumin-heme) with dioxygen and carbon monoxide. *Macromol. Symp. 195*, 275−280.

(21) (a) Collman, J. P., Brauman, J. I., Collins, T. J., Iverson, B. L., Lang, G., Pettman, R. B., Sessler, J. L., and Walters, M. A. (1983) Synthesis and characterization of the "pocket" porphyrins. *J. Am. Chem. Soc. 105*, 3038−3052. (b) Collman, J. P., Basolo, F., Bunnenberg, E., Collins, T. C., Dawson, J. H., Ellis, P. E., Marrocco, M. L., Moscowitz, A., Sessler, J. L., and Szymanski, T. (1981) Use of magnetic circular dichroism to determine axial ligation for some sterically encumbered iron(II) porphyrin complexes. *J. Am. Chem. Soc. 103*, 5636−5648.

(22) Komatsu, T., Matsukawa, Y., and Tsuchida, E. (2000) Kinetics of CO and O_2 binding to human serum albumin-heme hybrid. *Bioconjugate Chem. 11*, 772−776.

(23) Sumi, A., Ohtani, W., Kobayashi, K., Ohmura, T., Yokoyama, K., Nishida, M., and Suyama, T. (1993) Purification and physico-chemical properties of recombinant human serum albumin. *Biotechnology of Blood Proteins* (Rivat, C., Stoltz, J.-F., Eds.) Vol. 227, pp 293−298, John Libbey Eurotext, Montrouge.

Poly(ethylene glycol)-Conjugated Human Serum Albumin Including Iron Porphyrins: Surface Modification Improves the O_2-Transporting Ability

Yubin Huang,[†] Teruyuki Komatsu,[†,*] Rong-Min Wang,[†,‡] Akito Nakagawa,[†] and Eishun Tsuchida[†,*]

Advanced Research Institute for Science and Engineering, Waseda University, 3-4-1 Okubo, Shinjuku-ku, Tokyo 169-8555 Japan, and Key Laboratory of Polymer Materials of Gansu Province, Institute of Polymer, Northwest Normal University, Lanzhou 730070, China. Received November 3, 2005; Revised Manuscript Received February 10, 2006

Artificial O_2-carrying hemoprotein composed of human serum albumin including tetrakis(o-amidophenyl)-porphinatoiron(II) (Fe4P or Fe3P) [HSA−FeXP] has been modified by maleimide- or succinimide-terminated poly(ethylene glycol) (PEG), and the formed PEG bioconjugates have been physicochemically characterized. 2-Iminothiolane (IMT) reacted with the amino groups of Lys to create active thiol groups, which bind to α-maleimide-ω-methoxy PEG [Mw: 2-kDa (PEG$_{M2}$), 5-kDa (PEG$_{M5}$)]. On the other hand, α-succinimidyl-ω-methoxy PEG [Mw: 2-kDa (PEG$_{S2}$), 5-kDa (PEG$_{S5}$)] directly binds to Lys residues. MALDI-TOF MS of the PEG-conjugated HSA−FeXP showed distinct molecular ion peaks, which provide an accurate number of the PEG chains. In the case of PEG$_{MY}$(HSA−FeXP), the spectroscopic assay of the thiol groups also provided the mean of the binding numbers of the polymers, and the degree of the modification was controlled by the ratio of [IMT]/[HSA]. The viscosity and colloid osmotic pressures of the 2-kDa PEG conjugates (phosphate-buffered saline solution, [HSA] = 5 g dL^{-1}) were almost the same as that of the nonmodified one, whereas the 5-kDa PEG binding increased the rheological parameters. The presence of flexible polymers on the HSA surface retarded the association reaction of O_2 to FeXP and stabilized the oxygenated complex. Furthermore, PEG$_{MY}$(HSA−FeXP) exhibited a long circulation lifetime of FeXP in rats (13−16 h). On the basis of these results, it can be concluded that the surface modification of HSA−FeXP by PEG has improved its comprehensive O_2-transporting ability. In particular the PEG$_{MY}$(HSA−FeXP) solution could be a promising material for entirely synthetic O_2-carrying plasma expander as a red cell substitute.

INTRODUCTION

Poly(ethylene glycol) (PEG) is commonly used for the surface modification of peptides, proteins, enzymes, and liposome to confer several potential beneficial effects: not only a longer plasma half-life and nonimmunogenicity but also a solubility in organic solvents and extreme thermostability (1−4). To develop an artificial O_2 carrier, substantial efforts have been directed to the preparation of PEG-conjugated hemoglobin (Hb) over the past decades (5−8), and the optimized PEG−Hbs are currently being tested in clinical trials. Human serum albumin (HSA) is a versatile protein, which is found in our blood plasma at a high concentration (4−5 g dL^{-1}) (9). We have reported that HSA including tetrakis(o-amidophenyl)porphinatoiron(II) (Fe3P or Fe4P, Chart 1) [HSA−FeXP] can reversibly bind and release O_2 under physiological condition (pH 7.4, 37 °C) in a fashion similar to Hb (10). The administration of this synthetic O_2 carrier into anesthetized rats has proved its safety and O_2-transporting efficacy (11). Nevertheless, there is only one defect in that the FeXP molecule easily dissociates from HSA when infused into animals. This is due to the fact that FeXP is noncovalently bound to the hydrophobic cavity of albumin with binding constants (K) of 10^4-10^6 (M^{-1}). Natural heme, namely protoporphinatoiron IX, is also incorporated into HSA and shows a 10^2-10^4-fold higher K compared to FeXP (12); however, it is released from HSA during blood circulation with a half-life of 2.5−3.6 h (13, 14). Under these circumstances,

Chart 1. Structures of O_2-Adduct Complexes of Tetrakis-(o-amidophenyl)porphinatoiron(II)

Fe4P

Fe3P
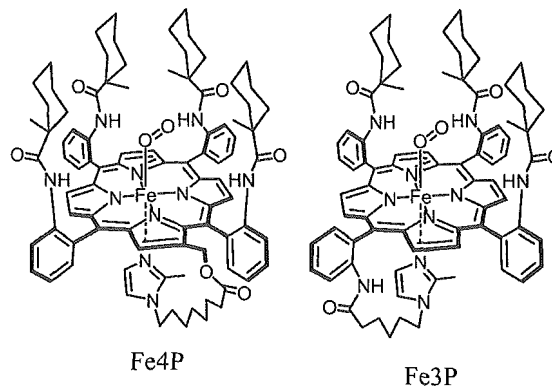
we postulated that the surface modification of HSA−FeXP by PEG could help to prolong the circulation life of FeXP and thereby retain its O_2-transporting ability for a long period. Although HSA is a very common plasma protein, its PEG conjugation chemistry has not yet been studied in detail. It is known that a huge variety of drugs are incorporated into specific sites of HSA (9). The PEG modification should prevent the rapid release of these drugs from the HSA scaffold and contribute to raising their potential therapeutic efficacies.

In the present study, we have systematically prepared several PEG-conjugated HSA−FeXPs and characterized their physicochemical properties. The surface modification by PEG affects the viscosity and colloid osmotic pressure of the solution, O_2-binding behavior of the parent HSA−FeXP, and circulatory lifetime of FeXP. The PEG-conjugated HSA−FeXP could be

* Corresponding authors: (E.T.) Tel: +81-3-5286-3120, Fax: +81-3-3205-4740, E-mail: eishun@waseda.jp. (T.K.) E-mail: teruyuki@waseda.jp; eishun@waseda.jp.

† Waseda University.

‡ Northwest Normal University.

of extreme medical importance as a red cell substitute or O_2-therapeutic reagent.

EXPERIMENTAL PROCEDURES

Materials and Apparatus. All reagents were purchased from commercial sources as special grades and used without further purification. 2-Iminothiolane hydrochloride (IMT) was purchased from Wako Pure Chemical Industries, Ltd. (Osaka, Japan). α-[3-(3-Maleimido-1-oxopropyl)amino]propyl-ω-methoxy PEG [averaged Mw: 2333 (Sunbright ME-020MA, PEG_{M2}), averaged Mw: 5207 (Sunbright MEMAL-50H, PEG_{M5})] and α-succinimidyloxyglutaryl-ω-methoxy PEG [averaged Mw: 2325 (Sunbright MEGC-20HS, PEG_{S2}), averaged Mw: 5261 (Sunbright MEGC-50HS, PEG_{S5})] were purchased from NOF Corp. (Tokyo, Japan). 2-{8-(2-Methylimidazolyl-1-yl)-octanoyloxymethyl}-5,10,15,20-tetrakis{α,α,α,α-o-(1-methylcyclohexanamido)phenyl}porphinatoiron(III) chloride (Fe4P) and 5,10,15-tris{α,α,α-o-(1-methylcyclohexanamido)-phenyl}-20-mono-[β-o-{6-(2-methylimidazolyl) hexanamido}-phenyl]porphinatoiron(III) chloride (Fe3P) were synthesized using previously reported procedures (*10d,e*). Recombinant HSA was provided by the NIPRO Corp. (Osaka, Japan). The UV−vis absorption spectra were recorded using an Agilent 8453 UV−visible spectrophotometer fitted with an Agilent 89090A temperature control unit. The water was deionized using Millipore Elix and Simpli Lab-UV.

Preparation of PEG-Conjugated HSA−FeXP. The HSA−FeXP solutions (X = 3, 4, [HSA]: 5 g dL^{-1}, [FeXP]/[HSA]= 4 (mol/mol), pH 7.4) were prepared as described elsewhere (*10b,d*).

PEG_{MY}(HSA−FeXP): The modification of HSA−FeXP by α-maleimide-ω-methoxy PEG_{M2} was, for instance, carried out as follows. IMT (72 mg, 0.54 mmol) was slowly added to the HSA−FeXP solution (48 mL, [HSA]: 5 g dL^{-1}, [Fe4P] = 3 mM, pH 7.4) ([IMT]/[HSA] = 15/1, mol/mol) and gently stirred at room temperature in the dark. After 3 h, PEG_{M2} (1.44 g, [PEG_{M2}]/[HSA]:20/1, mol/mol) was added to the mixture, which was continually stirred for another 2 h. The resultant solution was ultrafiltered and washed by at least a 600 mL of phosphate-buffered saline (PBS) solution (pH 7.4) to remove any unreacted IMT and PEG_{M2} using the ADVANTEC UHP-76K holder with a Q0500 076E membrane (cutoff Mw: 50 kDa). The volume was finally condensed to 48 mL and sterilized by a DISMIC 0.45 μm filter, producing the PEG_{M2}(HSA−FeXP) solution. The FeXP concentration was determined by the assay of the iron ion by inductively coupled plasma (ICP) spectrometry using a Seiko Instruments SPS 7000A Spectrometer. The HSA concentration was calculated from the intensity of the circular dichroism spectrum at 208 nm, because the molar ellipticity of HSA (1.9 × 10^4 deg cm^2 $dmol^{-1}$) was unaltered after the PEG conjugation. Circular dichroism (CD) spectra were obtained using a JASCO J-725 spectropolarimeter. The concentration of the HSA sample was 0.15 μM in PBS, and quartz cuvettes with a 10-mm thickness were used for the measurements over the range of 195−250 nm. The PEG_{M2}(HSA−Fe3P) and PEG_{M5}-(HSA−Fe4P) solutions were also prepared by the same procedure. The product was sealed in a glass bottle under CO pressure and stored at 4 °C.

PEG_{SY}(HSA−Fe4P): The surface modification of HSA−Fe4P by α-succinimidyl-ω-methoxy PEG_{S2} was carried out as follows. PEG_{S2} (0.72 g, 0.36 mmol) was directly added to the HSA−Fe4P solution ([HSA]: 5 g dL^{-1}, [Fe4P] = 3 mM, pH 7.4) ([PEG_{S2}]/[HSA]:10/1, mol/mol), and the mixture was stirred at room temperature for 2 h. The resultant solution was ultrafiltered, condensed (48 mL), and sterilized as described above, producing the PEG_{S2}(HSA−Fe4P) solution. Using PEG_{S5} instead of PEG_{S2}, PEG_{S5}(HSA− Fe4P) was obtained. The Fe4P

and HSA concentrations were determined by the same procedures for PEG_{MY}(HSA−FeXP).

Matrix-Associated Laser Desorption Ionization Time-of-Flight Mass Spectra (MALDI-TOF MS). The MALDI-TOF MS were obtained using a Shimadzu/Kratos AXIMA-CFR S/W Version 2, which was calibrated by BSA (Sigma A-0281) and HSA (Sigma A-3782). The specimens were prepared by mixing the aqueous sample solution (10 μM, 1 μL) and matrix (10 mg mL^{-1} sinapinic acid in 40% aqueous CH_3CN, 1 μL) on the measuring plate and air-drying.

Determination of Mean of PEG_{MY} Chains per Protein by Assay of Thiol Groups. The active thiol groups on the protein surface can be assayed by the disulfide exchange reaction with 2,2′-dithiopyridine (2,2′-DTP) to produce 2-thiopyridinone (2-TP) with an absorption at 343 nm (molar absorption coefficient (ϵ_{343}): 8.1 × 10^3 M^{-1} cm^{-1}) (*15*). Quantitative spectroscopic measurements conveniently provide the thiol concentration. The parent HSA−FeXP showed a small absorption band in this range, which should be subtracted from the spectrum after the disulfide exchange reaction. The difference in the thiol groups per HSA−FeXP before and after the PEG_{MY} modification corresponds to the mean of the PEG_{MY} chains on the protein surface.

Solution Properties. The viscosity and density of the PEG-conjugated HSA−FeXP solution (PBS, pH 7.4) were obtained using an Anton Paar DSC 300 capillary viscometer at 37 °C. The colloid osmotic pressures of the solutions (PBS, pH 7.4) were measured by a WESCOR 4420 Colloid Osmometer at 25 °C. A membrane filter with a 30 kDa cutoff was used.

O_2-Binding Parameters. O_2-binding to PEG-conjugated HSA−FeXP was expressed by eq 1,

$$PEG(HSA-FeXP) + O_2 \underset{k_{off}}{\overset{k_{on}}{\rightleftharpoons}} PEG(HSA-FeXPO_2) \quad (1)$$
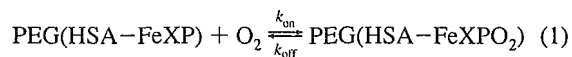
where $K = k_{on}/k_{off}$. The O_2-binding affinity (gaseous pressure at half O_2 binding for FeXP, $P_{1/2}$ = 1/K) was determined by spectral changes at various partial pressures of O_2/N_2 as previously reported (*10b,d*). The FeXP concentrations of 10−20 μM were normally used for the UV−vis absorption spectroscopy. The spectra were recorded within the range of 350−700 nm. The half-lifetime of the O_2-adduct complex was determined by the time dependence of the absorption intensity at 550 nm (O_2-adduct species). The association and dissociation rate constants for O_2 (k_{on}, k_{off}) were measured by a competitive rebinding technique using a Unisoku TSP-1000WK laser flash photolysis as reported in a previous paper (*16*).

Circulation Lifetime in Vivo. The animal investigations were carried out using twenty male Wistar rats (297 ± 29 g). All animal handling and care were in accordance with the NIH guidelines. The protocol details were approved by the Animal Care and Use Committee of Keio University. The PEG-conjugated HSA−FeXP solution (20% volume of the circulatory blood) was intravenously injected into rats from the tail vein (1 mL/min) under an inhalation anesthesia with diethyl ether (n = 4 each). Blood was taken from the tail vein at 3, 30 min, 1, 2, 4, 8, 16 h, 1, 2, 3 days (10 time points) after the infusion and then centrifuged to isolate the serum, which was colored brown by the presence of the sample. The animals were sacrificed after the experiments by hemorrhage. The FeXP concentration was measured by an iron ion assay using ICP spectrometry as described above.

RESULTS AND DISCUSSION

Synthesis of PEG-Conjugated HSA−FeXP. The HSA−FeXP molecules were conjugated with PEG having a terminal reactive chain-end, maleimide-PEG or succinimide-PEG, at
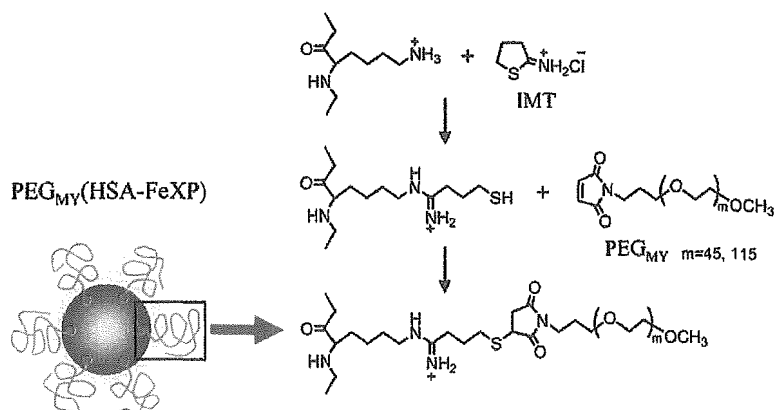
Figure 1. Two-step reaction schemes of IMT and maleimide-PEG (PEG$_{MY}$) with HSA−FeXP.

ambient temperature. Thiolation regent, IMT, quantitatively reacted with the amino groups of Lys to create active thiol groups, which bind to the α-maleimide-ω-methoxy PEG (PEG$_{M2}$ or PEG$_{M5}$) (Figure 1). The two-step reaction is reproducible and did not form any toxic side-product. On the other hand, the α-succinimidyl-ω-methoxy PEG (PEG$_{S2}$ or PEG$_{S5}$) directly binds to the amino groups of Lys. The gel permeation chromatogram (Sephacryl 200HR) of the well-washed PEG conjugate exhibited a single band, so that we did not need any further chromatographic purification.

The MALDI-TOF MS of PEG$_{M5}$(HSA−Fe4P), as prepared under the condition of [IMT]/[HSA−Fe4P] = 15/1 (mol/mol), showed five distinct ion peaks at 85, 90, 95, 101, and 106 kDa (Figure 2a). No unreacted HSA−FeXP was observed at all. The difference in each mass was 5.25 kDa, which implies that HSA−Fe4P is covalently bound to PEG$_{M5}$ and the individual peaks are attributed to PEG$_{M5}$(HSA−Fe4P) having a different number of PEG chains. Here, we have to be cautious whether these mass values involve a molecular weight of Fe4P, because our previous MALDI-TOF MS experiments of HSA−Fe4P demonstrated a single peak of HSA (Mw: 66.5 kDa); the incorporated Fe4P dissociated from the albumin during the ionization process (10a). In this study, we found that the mean of the surface PEG chains on HSA−FeXP is conveniently determined by a spectroscopic assay of the HSA scaffold and thiol groups. In general, the concentration of HSA is measured by the absorption at 280 nm or bromcresol green method (17), but they are probably obstructed by the surface modification. We then employed a CD measurement to determine the HSA concentration. The comparison of the CD spectra of HSA and PEG−HSA solutions revealed that the molecular ellipcity of albumin (ϵ_{208} = 1.9 × 10^4 deg cm^2 dmol^{-1}) is unaltered even after the PEG binding. Moreover, the presence of FeXP does not disturb the CD in the range of 190−250 nm. Therefore, the HSA concentration of PEG modified HSA−FeXP was quantitatively determined by its CD intensity at 208 nm. On the other hand, the active thiol groups on proteins are generally assayed by a disulfide exchange reaction with 2,2′-DTP (15). The combination of these two methodologies allows us to estimate the number of thiols on HSA−FeXP. The mean of the thiol groups was 6.7 per protein after the thiolation by IMT ([IMT]/[HSA−Fe4P] = 15 mol/mol) and decreased to 0.6 after the reaction with 20-fold excess moles of PEG$_{M5}$ (Table 1). These results suggested that the mean of 6.1 reactive thiols was conjugated with PEG$_{M5}$. The averaged molecular weight of this PEG$_{M5}$(HSA−FeXP) calculated from the intensity of the MS peak was 95 kDa. If one subtracts the total mass of the six PEG$_{M5}$ chains (5 kDa × 6 = 30 kDa) from 95 kDa, the difference of 65 kDa equals that
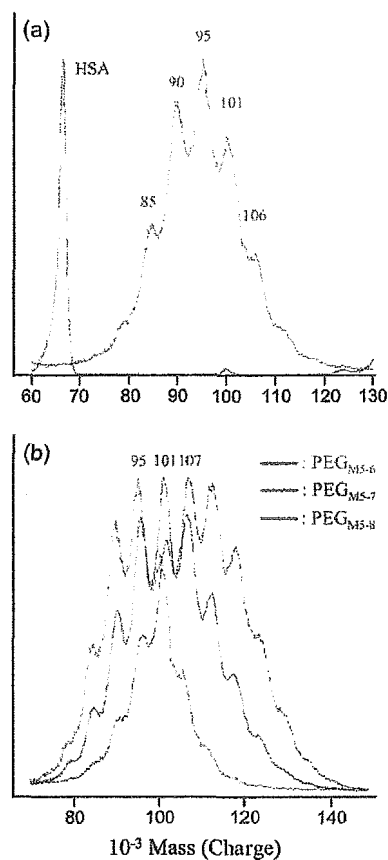

Figure 2. MALDI-TOF MS of (a) HSA and PEG$_{M5-6}$(HSA−Fe4P) and (b) PEG$_{M5}$(HSA−Fe4P) prepared in different [IMT]/[HSA−Fe4P] ratios of 15 (red), 20 (blue), and 30 (green) (mol/mol).

of HSA without Fe4P. Therefore, we concluded that all the mass ion peaks observed in the MALDI-TOF MS did not include the molecular weight of FeXP.

The number of the meleimide-PEG$_{M5}$ chains on HSA−Fe4P were modulated by the mixing ratio of [IMT]/[HSA−Fe4P] (mol/mol). The maximum peak of PEG$_{M5}$(HSA−Fe4P) in the MALDI-TOF MS significantly shifted to the higher molecular region (95 → 101 → 107 kDa) by increasing the IMT (Figure 2b). It is quite remarkable that the distributions of the entire spectral pattern were always identical. The averaged binding number of the PEG$_{M5}$ chains per HSA estimated from the intensity of the mass peak was consistent with the number determined from the assay of the thiol groups (Table 1).